RSC Advances

REVIEW

View Article Online
View Journal | View Issue

Cite this: *RSC Adv.*, 2022, **12**, 17959

Strategies to improve electrocatalytic performance of MoS_2-based catalysts for hydrogen evolution reactions

Xinglong Zhang,[a] Shiying Hua,[b] Long Lai,[a] Zihao Wang,[a] Tiaohao Liao,[a] Liang He,[c] Hui Tang *[a] and Xinming Wan*[d]

Received 16th May 2022
Accepted 13th June 2022

DOI: 10.1039/d2ra03066g

rsc.li/rsc-advances

Electrocatalytic hydrogen evolution reactions (HERs) are a key process for hydrogen production for clean energy applications. HERs have unique advantages in terms of energy efficiency and product separation compared to other methods. Molybdenum disulfide (MoS_2) has attracted extensive attention as a potential HER catalyst because of its high electrocatalytic activity. However, the HER performance of MoS_2 needs to be improved to make it competitive with conventional Pt-based catalysts. Herein, we summarize three typical strategies for promoting the HER performance, *i.e.*, defect engineering, heterostructure formation, and heteroatom doping. We also summarize the computational density functional theory (DFT) methods used to obtain insight that can guide the construction of MoS_2-based materials. Additionally, the challenges and prospects of MoS_2-based catalysts for the HER have also been discussed.

1. Introduction

With the rapid growth of the economy, the traditional, polluting sources of energy are being consumed heavily, resulting in environmental degradation;[1–3] thus, developing sustainable and clean energy has become urgent. Among all the alternative energies, hydrogen has significant advantages due to its high energy density and environmental friendliness.[4] Currently, mass H_2 production mainly comes from steam reforming of hydrocarbons, which is highly energy-consuming and relies on the polluting petroleum industry.[5–7] To promote the adoption of the H_2 economy, in the past several decades, new H_2 production technologies, like photocatalytic and electrocatalytic water splitting, have been developed.[8–12] Compared with photocatalytic water splitting, the electrochemical approach has more advantages in terms of energy efficiency and achieving effective product separation. Electrochemical water splitting consists of two half-reactions, which are named as the hydrogen evolution reaction (HER) and oxygen evolution reaction (OER).[13] The OER is hard to occur, because it involves four-electron transfer.[14] The reaction mechanism is as follows:

Total reaction:

$$H_2O(l) \rightarrow H_2(g) + \frac{1}{2}O_2(g) \quad (1)$$

In acidic solution:

$$\text{Cathode: } 2H^+(aq) + 2e^- \rightarrow H_2(g) \quad (2)$$

$$\text{Anode: } H_2O(l) \rightarrow 2H^+(aq) + \frac{1}{2}O_2(g) + 2e^- \quad (3)$$

In neutral and alkaline solution:

$$\text{Cathode: } 2H_2O(l) + 2e^- \rightarrow H_2(g) + 2OH^-(aq) \quad (4)$$

$$\text{Anode: } 2OH^-(aq) \rightarrow H_2O(l) + \frac{1}{2}O_2(g) + 2e^- \quad (5)$$

Generally, the HER consists of the three following steps:

$$\text{Volmer step: } H^+ + e^- \rightarrow H^* \quad (6)$$

$$\text{Heyrovsky step: } H^* + H^+ + e^- \rightarrow H_2 \quad (7)$$

$$\text{Tafel step: } 2H^* \rightarrow H_2 + 2^* \quad (8)$$

In acidic electrolytes, the HER occurs when protons are adsorbed at the surface of the MoS_2 and consequently, step (6) takes place, which is then followed by step (7) or (8). The overall reaction rate relies on the Gibbs free energy of H_2 adsorption (ΔG_{H^*}). In theory, the closer this value is to zero, the greater is the HER activity. The reactions (7) or (8) are inhibited when the binding of H to the catalyst surface is weak. Therefore, catalysts

[a]*School of Materials and Energy, University of Electronic Science and Technology of China, Chengdu, 611731, P. R. China. E-mail: tanghui@uestc.edu.cn; wanxinmin@caeri.com.cn*

[b]*Wuhan Institute of Marine Electric Propulsion, Wuhan 430064, P. R. China*

[c]*School of Mechanical Engineering, Sichuan University, Chengdu 610065, P. R. China*

[d]*China Automotive Engineering Research Institute Co., Ltd., Chongqing 401122, P. R. China*

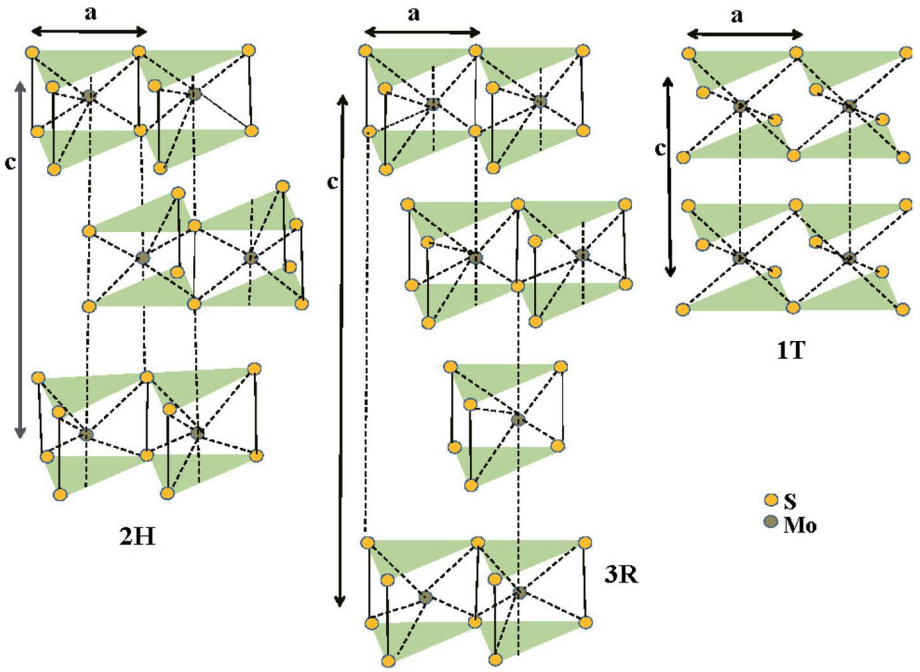

Fig. 1 Structural polytypes of MoS_2:1T, 2H, and 3R. Reproduced with permission from ref. 51. Copyright 2020, Elsevier.

with excellent HER performance tend to exhibit good adsorption of H atoms, which is conducive to charge transfer and bond breakage, resulting in the formation of H_2.[9,15–18]

Under standard conditions, initiating HER requires a dynamic overpotential, which essentially involves additional energy consumption; thus, electrocatalysts are integral to abate the overpotential. As of today, Pt-based materials are the most widely used electrocatalysts; however, Pt is scarce and costly, making it essential to develop cost-effective electrocatalysts. Currently, a wide range of materials, including transition metal alloys,[19–27] transition metal carbides,[28–36] transition metal dichalcogenides,[37–45] transition metal phosphides,[46–50] and so on, are being studied as possible alternative HER electrocatalysts. Among them, MoS_2 has attracted wide attention due to its unique two-dimensional layered structure and adjustable band gap width, which makes MoS_2 has a property of ease incorporation into the lattice (heteroatoms and vacancies) and adjustability of electron transport. However, experimental and theoretical studies reveal that the HER activity of MoS_2 remains unsatisfactory due to three main issues. First, the HER activity of MoS_2 correlates with the active edge sites rather than basal planes, but the edge sites just account for a small part of the surface area of MoS_2. Second, the semiconducting basal plane of MoS_2 has a low intrinsic electronic conductivity, which leads to poor charge transfer. Third, the aggregation and restacking of MoS_2 hinders the availability of edge sites. Herein, we discuss three important approaches that have been demonstrated to improve the intrinsic catalytic activity and HER performance of MoS_2 effectively, *i.e.*, defect engineering, formation of the heterostructure, and heteroatom doping (Fig. 1).

2. Properties of MoS_2

MoS_2 is a typical layered transition metal dichalcogenides composed of stacking S–Mo–S layers by van der Waals interactions, leading to a sandwich-like layered structure.[51,52] The basal plane of MoS_2 is generally believed to be inert toward HER, while the edge sites of MoS_2 layers possess much higher chemical reactivity than the basal plane.[13] Based on the arrangement of the S atoms, three phases of MoS_2 can be obtained, *i.e.*, 1T, 2H and 3R.[53] The 2H phase MoS_2 is thermodynamically stable, but the conductivity of 2H phase MoS_2 is poor.[54,55] Compared to 2H MoS_2, 1T MoS_2 is metallic and is 10^7 times more conductive than 2H MoS_2.[56] Nevertheless, 1T MoS_2 is thermodynamically unstable and does not exist in nature[57] (Fig. 2). Under some specific conditions,1T MoS_2 can also exist and phase transformation is one of the most effective methods to improve the catalytic performance of MoS_2.[58,59] Zhao *et al.*[60] investigated the HER dynamics in the MoS_2 basal plane of the 1T and 2H phases. They calculated the absorbed H free energies on the 2H/1T structural interfaces and their work offered a new way to increase the number of MoS_2 active sites on the basal plane. DFT calculations demonstrated that MoS_2 had a similar H binding energy as that of Pt.[61] In theory, MoS_2 should exhibit outstanding HER performance; however, bulk MoS_2 displays poor performance due to the following reasons. (i) The active sites of bulk MoS_2 cannot be fully exposed.[62] (ii) The superimposition of the van der Waals force in the interior of the bulk MoS_2 leads to an incongruous effect of the active sites.[63] (iii) The covalently bonded atoms in the layers lead to poor HER performance.[64] (iv) The electronic conductivity of bulk MoS_2 is low.[65] Thus, many efforts have been devoted to designing

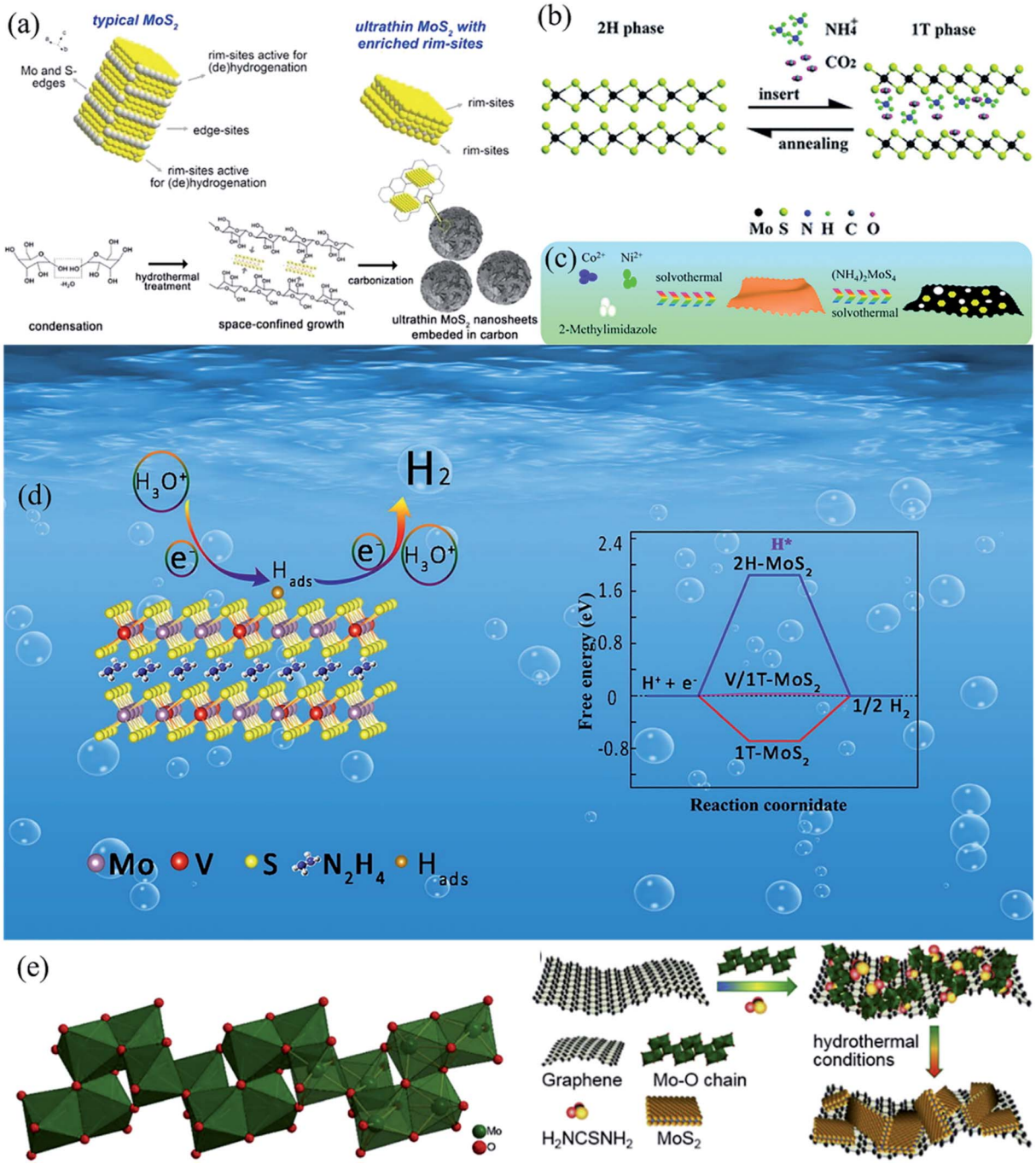

Fig. 2 (a) Schematic illustration for synthesis of MoS_2/C. Reproduced with permission from ref. 116, Copyright 2014 Elsevier. (b) Schematic illustration of 1T/2H MoS_2 phase transition. Reproduced with permission from ref. 117, Copyright 2017 Royal Society of Chemistry. (c) Schematic of the synthesis process for MoS_2/NiCoS heterostructures. Reproduced with permission from ref. 118, Copyright 2019 Royal Society of Chemistry. (d) Schematic illustration of HER process and DFT calculation results. Reproduced with permission from ref. 119, Copyright 2021 Elsevier. (e) Molybdenum oxide chain in $(H_2en)Mo_3O_{10}$ and the proposed formation mechanism of 1T/2H-MoS_2/RGO. Reproduced with permission from ref. 120, Copyright 2021 Elsevier.

a reasonable MoS_2 nanostructure and modulating the MoS_2 electronic structure.[66–68] Furthermore, many engineering methods such as phase transformation engineering, vacancy engineering, and stretching have been developed to overcome the disadvantages of bulk MoS_2.[69–73] Cao *et al.*[74] demonstrated that S vacancies could provide another type of active site for the HER besides the Mo and S active edge sites. They also found that the HER activity of grain boundaries was much lower than that of the S vacancy and S edge sites. Based on the structure determining properties, many efforts have been devoted to constructing specific MoS_2 nanostructures, including nanoparticles, nanoflakes, nanowires, nanoflowers and

nanosheets.[75–79] These nanostructures can maximally expose active edge sites of MoS_2 and shorten the electron transfer distance.[80]

3. Synthetic methods for MoS_2

In order to synthesize MoS_2, many strategies have been developed, including mechanical exfoliation,[81–83] solution exfoliation,[84–86] chemical vapor deposition[87–89] (CVD), hydrothermal synthesis,[90–92] electrodeposition methods,[93–95] metal–organic chemical vapor deposition (MOCVD),[96–98] and molecular beam epitaxy (MBE).[99–101] These methods can be classified as top-down methods (including mechanical exfoliation and solution exfoliation) and bottom-up methods (including hydrothermal synthesis, CVD, MOCVD and MBE). In the top-down methods, the morphology of MoS_2 can be well controlled since the structure of the final product is inherited from the original materials.[102] However, top-down methods have intrinsic shortcomings; for instance, the nanoscale morphology of the final product is hard to adjust since it is difficult to change the distance between ions and atoms in top-down methods.[103] In bottom-up methods, a large and complicated system are formed by atoms, molecules and nanoparticles through self-assembly or weak interactions, and the usage of materials is more efficient.[104] The specific surface area and thickness of MoS_2 can be better controlled than in top-down methods. For example, in hydrothermal method, the thickness and size of MoS_2 can be modulated by simply tuning the hydrothermal time, temperature and growth parameters of solution concentration.[105] The main disadvantage of bottom-up methods is the difficulty of large-scale synthesis.[106,107] In the rest of this section, we try to list out the general methods of synthesizing MoS_2 for the electrochemical HER (Table 1).

3.1. Hydrothermal synthesis

Hydrothermal method is to seal the reactants in the reactor, and the reaction process is completed through chemical transmission. Liquid or gaseous water is the pressure transmission medium under high temperature and high pressure, and most of the reactants can be dissolved in water, so that the reaction can be carried out in the critical state of gas phase and liquid phase solvent. Compared with other powder preparation methods, the powder prepared by hydrothermal methods has the advantages of complete grain development, small particle size, uniform distribution, light particle agglomeration, cheaper raw materials, and appropriate stoichiometry and crystal shape are easily obtained.[108–111] Typically, the ceramic powder prepared by hydrothermal methods does not need high-temperature calcination treatment, which prevents grain growth, defect formation and introduction of impurities in the calcination process, so the prepared powder has high sintering activity.[112–115]

Liu *et al.*[116] prepared ultrathin MoS_2 nanosheets grown on an *in situ*-formed polysaccharide matrix derived from glucose condensation *via* a hydrothermal method. 0.80 g of glucose with a varied amount of ammonium heptamolybdate tetrahydrate ($(NH_4)_6Mo_7O_{24}\cdot 4H_2O$) and thiourea ($CS(NH_2)_2$) was dissolved in 15.0 mL of distilled water, and then the solution was turned to a Teflon-lined stainless-steel autoclave, with a hydrothermal treatment at 240 °C for 48 h. After centrifugation, washing and annealing, the MoS_2/C nanospheres was successfully synthesized. Wang *et al.*[117] prepared 1T/2H MoS_2 *via* a facile hydrothermal method with the addition of ammonium bicarbonate. During the hydrothermal process, ammonium bicarbonate was decomposed into small molecules and ions as guests, including NH_4^+, H_2O and CO_2, which were inserted into the lamellar structures of MoS_2, inducing the formation of multiphasic 1T/

Table 1 Comparison of synthetic methods of MoS_2-based catalysts

Synthetic method	Advantages	Disadvantages	Reference
Hydrothermal synthesis	Easy to operate, high purity, good dispersibility, complete crystal form, uniform particle size	Easy to agglomerate, unclear reaction mechanisms, unsuitable for water sensitive materials, poor repeatability	90–92
Chemical vapor deposition	Simple film-forming device, easy to control the product composition, good repeatability, good uniformity	May produce corrosive, toxic or explosive reaction gas, low film forming rate, easy to introduce impurities	87–89
Mechanical exfoliation	Few defects, smooth surface, high mobility	Difficult to control the thickness, random position on substrate, small output	81–83
Solution exfoliation	Low cost, high controllability, easy to realize large-scale preparation	Small product size, low yield	84–86
Electrodeposition methods	Adjustable grain size, easy to operate, low cost, high efficiency	Difficult to control growth rate, low crystallinity of product	93–95
Metal–organic chemical vapor deposition	Low reaction temperature, wide application range, suitable for mass production	May produce toxic and flammable vapor, difficult to *in situ* monitor the growth process	96–98
Molecular beam epitaxy	Atomic-level controlled film thickness, composition and dopants	High requirements for equipment conditions	99–101

2H MoS_2. Zhang *et al.*[118] used the hydrothermal method to construct MoS_2/NiCoS nanosheets with ultrathin NiCo bimetal–organic framework (NiCo-MOF) nanosheets and $(NH_4)_2MoS_4$ as precursors. The hydrothermal process was controlled at 200 °C for 24 h. In this reaction, $(NH_4)_2MoS_4$ not only acts as a precursor for the synthesis of MoS_2, but also provides a source of sulfur for *in situ* conversion of NiCo-MOF nanosheets to NiCoS. Li *et al.*[119] prepared V-doped 1T MoS_2 nanosheets as a highly efficient HER electrocatalyst in both acidic and alkaline solutions through a hydrothermal method. Typically, 0.2 g sulfur was put into 4 beakers with different molar quantity of ammonium heptamolybdate ($(NH_4)_6Mo_7O_{24}\cdot 4H_2O$). Then, 4 mL of hydrazine monohydrate ($N_2H_4\cdot H_2O$) was dissolved in each beaker. Then, 36 mL of DI water was added into the beakers to make the mixture 80% of autoclave volume, and different molar quantity of ammonium metavanadate (NH_4VO_3) were added into the beakers as the V source. Then the precursors were transferred to 50 mL stainless steel autoclaves. The whole set was sealed and put into the oven at 200 °C for 48 h. Xiao *et al.*[120] synthesized 1T/2H MoS_2@-graphene *via* a hydrothermal method. The introduction of metallic 1T-MoS_2 endues the as-prepared materials with remarkably electrocatalytic activity and favorable kinetics, highly efficient and stable HER performance.

3.2. Chemical vapor deposition

Chemical vapor deposition (CVD) is a method of synthesizing coatings and nanomaterials deposited on a substrate surface by chemical gas or vapor reaction. It is the most widely used technology for depositing a variety of materials in the semiconductor industry, including a wide range of insulating materials, most metal materials and metal alloy materials.[121–123] Theoretically, the CVD process is very simple: two or more gaseous raw materials are introduced into a reaction chamber, which then react with each other to form a new material that is deposited on the wafer surface. However, experimentally, the reaction that takes place in the reaction chamber is very complex, and there are many factors that must be considered. The deposition parameters, which can vary over a wide range, include the pressure in the reaction chamber, the temperature of the wafer, the flow rate of the gas, the distance of the gas through the wafer, the chemical composition of the gas, the ratio of one gas to another, the role of the intermediate product of the reaction, and whether other reactions are needed.[124–128]

Pumera *et al.*[129] synthesized MoS_2 films *via* powderless gas deposition. The CVD fabrication method they used is suitable for industry because this powderless and one-step process eliminates the deviations of MoS_2 growth which are likely to arise from the usage of a powder precursor. Yu *et al.*[130] hybridized MoS_2 micro-flowers on VS_2 by a one-pot CVD method and their catalyst exhibited excellent HER performance. Atomic layer deposition (ALD) is a method in which substances can be deposited on the surface of the substrate, layer by layer, in the form of a monoatomic film.[131] ALD has similarities with ordinary chemical deposition, except that the chemical reaction of the new layer of atomic film is directly dependent on the previous layer. In this way, only one layer of atoms is deposited per reaction. Due to its highly controllable deposition parameters (thickness, composition, and structure), atomic layer deposition technology, excellent deposition uniformity and consistency, it has wide application potential in the field of micro-nanoelectronics and nanomaterials. Tan *et al.*[132] successfully synthesized layered MoS_2 *via* the ALD method. Typically, MoS_2 films were prepared by alternating exposure to molybdenum chloride ($MoCl_5$) and hydrogen disulfide (H_2S) vapors. Due to the self-limiting reactions of the vapors, the number of MoS_2 film layers can be precisely controlled by the number of deposition cycles.

3.3. Exfoliation method

At present, the most effective preparation methods of single- or few-layer MoS_2 are exfoliation methods, which can be divided into mechanical exfoliation, lithium-ion intercalation exfoliation and liquid phase ultrasonic exfoliation. In the mechanical exfoliation method, MoS_2 powder is directly stripped to form a thin layer of MoS_2 nanoflakes with a special gummed tape. This is the most original and traditional preparation method. The thickness of MoS_2 that was first peeled off in 1965 ranged from a few layers to dozens of layers.[133] After the improvement of this stripping process, monolayer MoS_2 was successfully obtained.[134] The most obvious advantage of the mechanical exfoliation method is that the process is simple, can be obtained manually, and the stripping efficiency is high. Since this is direct exfoliation, the monolayer MoS_2 can maintain a good single crystal structure and offer high carrier mobility. However, this method has obvious disadvantages, such as low yield and poor repeatability. The lithium-ion intercalation-based exfoliation method can be used, for instance the Li_xMoS_2 ($x \geq 1$) intercalation compound is obtained by the reaction of the lithium-ion intercalation agent (such as *n*-butyl lithium) and MoS_2 powder (intercalation process). Then the intercalation compound reacts violently in water and other protonic solvents, and the stripping process occurs. Thus, multilayer and monolayer MoS_2 can be obtained by ultrasonic extraction. In 1986, Morrison *et al.*[135] prepared monolayer MoS_2 by this method. The efficiency of the Li ion intercalation stripping was found to be very high, with a yield close to 100%. The quality of the prepared nanosheets was very good, making it suitable for mass-production, and the method could be used to peel many other inorganic layered compounds. However, this preparation method is complex, the intercalation agent is sensitive to the environment, leading to a high production cost, and long preparation time. Moreover, it is difficult to control the degree of intercalation, which makes the post-treatment difficult. For this reason, Zeng *et al.*[136] used an electrochemical lithium battery device to control the lithium ion insertion and stripping process, so as to prepare a variety of monolayer materials such as MoS_2. This electrochemical lithium-ion intercalation exfoliation method can effectively avoid many of the abovementioned problems and obtain high yield monolayer MoS_2. The basic principle of the liquid-phase ultrasonic exfoliation method is to put MoS_2 and other layered materials into a suitable solvent,

use the ultrasonic wave to vibrate and peel off the lower layer of materials from the block, and then centrifuge to obtain thin MoS_2 nanosheets. In 2011, Coleman *et al.*[137] prepared monolayer and multilayer nanosheets such as MoS_2, BN and WS_2. The solvent selected by the liquid phase ultrasonic exfoliation method is generally a polar solvent with good dispersity

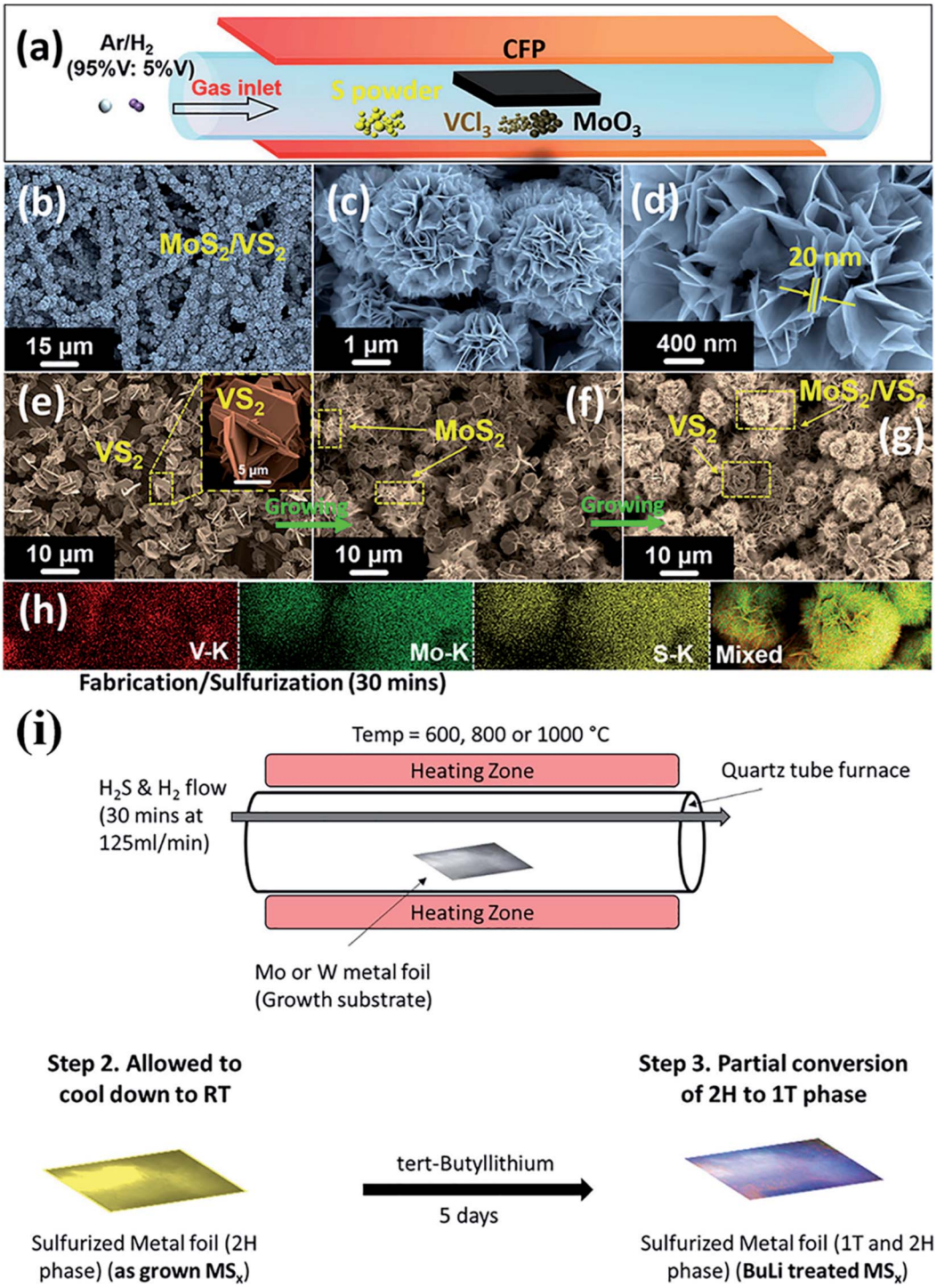

Fig. 3 (a) Schematic diagram of preparing MoS_2/VS_2 hybrid by a one-pot CVD process. The SEM images of MoS_2/VS_2 hybrid observed at different magnifications. (b) Low magnification; (c) middle magnification; and (d) high magnification. The morphological evolutions of MoS_2/VS_2 hybrid intercepted at different temperatures; (e) formation of pristine interfaced flake-like VS_2 crystals at 300 °C, with an inset shows the high-magnification of VS_2 crystals; (f) initial nucleation of flower-like MoS_2 on the existing VS_2 crystals at 730 °C; and (g) further growth of flower-like MoS_2 on underlying flake-like VS_2 crystals at 750 °C. (h) The EDX mapping of MoS_2/VS_2 hybrid, in which the elemental distributions of vanadium, molybdenum, and sulfur are illustrated in red, green, and yellow, respectively. Reproduced with permission from ref. 130, Copyright 2021 Elsevier. (i) Schematic illustration for a one-step powderless deposition growth process of 2H-MoS_2. Reproduced with permission from ref. 129, Copyright 2021 Elsevier.

and solubility for layered materials and similar surface energy. Coleman *et al.*[138] prepared thin MoS_2 material by adding a sodium cholate surfactant and stripping it in an aqueous phase. However, Zhou *et al.*[139] used ethanol/water mixed low-boiling solvents to successfully peel off nanosheets such as MoS_2, making the peeling method cheaper and environmentally friendly, and peeling MoS_2 under water phase conditions has become a new choice for people. The liquid-phase ultrasonic peeling method is simple and fast, and can be suitable for large-scale production, but generally the peeling degree is not high, the concentration of the obtained nanosheet solution is small, and the dependence on the ultrasonic conditions is high, and the ultrasonic power is too large or too small, which is not conducive to the formation of nanosheets.

3.4. Electrodeposition method

Electrodeposition method is an attractive way to synthesize MoS_2 thin film in large scale because it uses cheap equipment, enables the deposition in large area and easy control of growth parameters through applied potential, current, pH and temperature of the bath.[140] Many researchers have studied the mechanism of an electrochemical deposition of MoS_2 from aqueous and little from non-aqueous solutions. A variety of electrodeposition techniques have been reported for the preparation of MoS_2 films using anodic oxidation or cathodic reduction.

Ping *et al.*[141] developed an edge-guided electrodeposition approach for the construction of high quality edge contacted metal-2D MoS_2 and further demonstrated the potential of this approach in the fabrication of high performance electrocatalyst. Hwang *et al.*[142] developed a novel MoS_2 electrode with a nanocarbon (NC) coating as a catalytic cathode for hydrogen production in a microbial electrolysis cells (MEC), while treating simulated urine. The MEC performance of HER using the MoS_2-NC cathode was characterized and evaluated under different applied voltages and various dilution factors for adjusting conductivity. Lyndi *et al.*[143] prepared MoS_2 films *via* an electrodeposition method. Electrodeposition of molybdenum disulfide films was carried out with a 10 mM $(NH_4)_2MoS_4$ (ammonium tetrathiomolybdate) with 0.1 M $LiClO_4$ adjusted to pH 10 with NH_4OH using chronoamperometric deposition. Jiang *et al.*[144] prepared the MoS_2–Co_3S_4/NF heterostructure layer by Co-MOF vulcanization and cyclic voltammetry (CV) method, which showed better electrochemical performance than the single-layer Co_3S_4/NF. The as-prepared MoS_2–Co_3S_4 heterostructure layer was decorated by ZnCo-LDH, the hydrogen evolution performance was further improved.

Though the above synthetic methods have been demonstrated to be an effective way to synthesize bulk MoS_2, the HER performance of bulk MoS_2 is still not satisfactory. In the following part, we summarize three main strategies to promote the HER performance of MoS_2 (Fig. 3).

4. Main strategies to promote the HER performance of MoS_2

4.1. Defect engineering

Many physical and chemical properties of materials are closely related to the existence of defects.[145–147] Generally, defects can be classified as vacancies, grain boundaries and disorders.[148–150] Furthermore, vacancies can consist of, for instance, Mo vacancies, S vacancies, O vacancies, N vacancies and C vacancies.[151–155] Thermodynamically, it's unavoidable to introduce vacancies in the process of synthesizing MoS_2.[156] Many studies

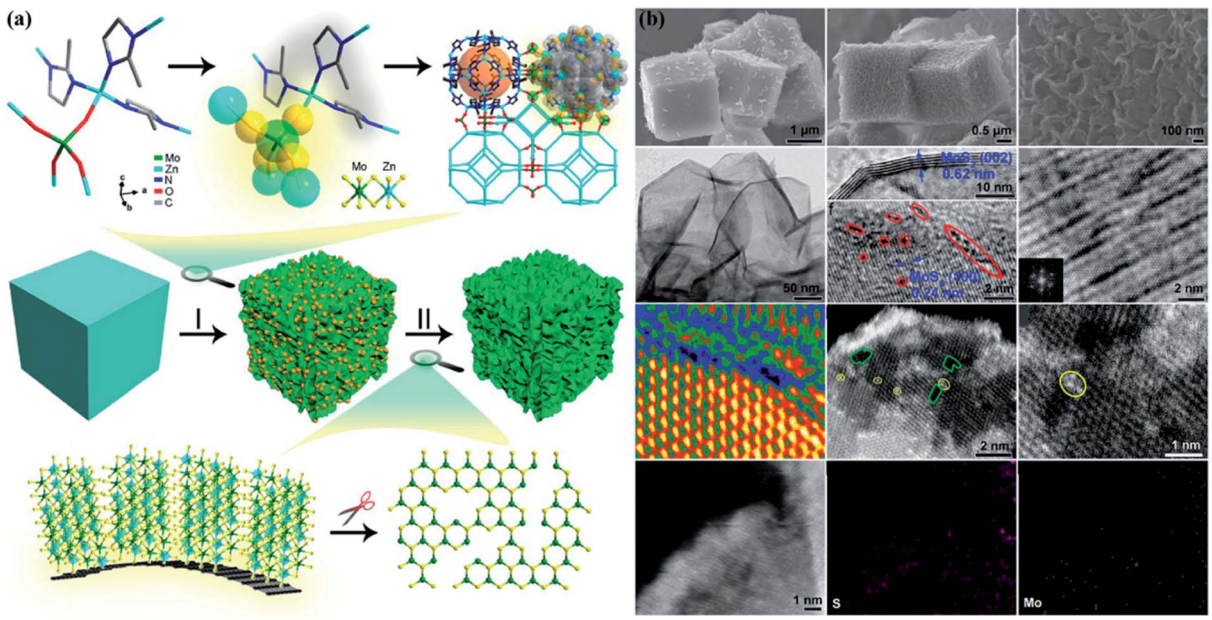

Fig. 4 (a) Schematic representation of the formation of c-MoS_2–C; (b) SEM images of HZIF-Zn/Mo and c-MoS_2–C. TEM image, HRTEM images, FFT-generated image of c-MoS_2–C. Atomic-resolution HAADF-STEM images of c-MoS_2–C with multiple Mo_xS_y vacancies. EDS elemental mapping for c-MoS_2–C. Reproduced with permission from ref. 168, Copyright 2021 American Chemical Society.

have examined the impact of vacancies on the HER performance of MoS_2.[157–167] Theoretically, the rational design of defects on the basal plane of MoS_2 can enhance the HER performance of MoS_2 because the basal plane of MoS_2 is inert while the edge sites are significantly more active.

Li *et al.*[168] designed vertically aligned MoS_2 with a selectively cleaved Mo–S bond. Their work showed a new way to synthesize MoS_2 with a vacancy and their synthesis route is shown in Fig. 4(a). Fig. 4(b) shows that the scanning electron microscopy (SEM) and transmission electron microscopy (TEM) images confirm the existence of micro-cubic c-MoS_2–C morphology. Aberration-corrected high-angle annular dark-field scanning transmission electron microscopy (AC HAADF-STEM) images show the existence of the vacancy. This unique defect is beneficial to a thermoneutral H-adsorption energy, which leads to accelerate HER kinetics. The energy-dispersive X-ray spectroscopy (EDS) elemental mapping results further confirm the formation of MoS_2 nanosheets with Mo and S defects. The electrocatalytic performance of the defect-rich MoS_2 is shown in Fig. 5. Further DFT calculations reveal that the newly generated interior edge sites break the periodic electronic structure of the MoS_2 basal plane, leading to an optimized surface charge configuration for H adsorption and desorption.

Li *et al.*[74] conducted a study of the catalytic activities of all potential reaction sites, such as edge sites, S vacancies and grain boundaries. For the first time, they demonstrated that S vacancies provide another active site for HER in addition to the well-known active edge sites (Fig. 6(a)). In order to identify the influence of S vacancy states and concentration on catalysis, Wang *et al.*[169] synthesized MoS_2 with homo-vacancies, with an H_2O_2 chemical etching strategy (Fig. 6(b)). They performed DFT calculations of ΔG_{H^*} to explore the effect of S vacancy concentration and distribution on the HER performance. The results showed that 12.50% of the single S-vacancies yielded the optimal HER performance. They synthesized a vertically aligned MoS_2 nanosheet guided by these theoretical DFT calculations. The X-ray diffraction (XRD) results in Fig. 7(a) demonstrate that the sample phase was firm and did not change after H_2O_2 etching. To determine the S-vacancy concentration as a function of the etching process, three X-ray photoelectron spectroscopy (XPS) spectra of P-MoS_2 and MoS_{2-x} are shown in Fig. 7(a). The S : Mo ratio in each spectrum was calculated and it was

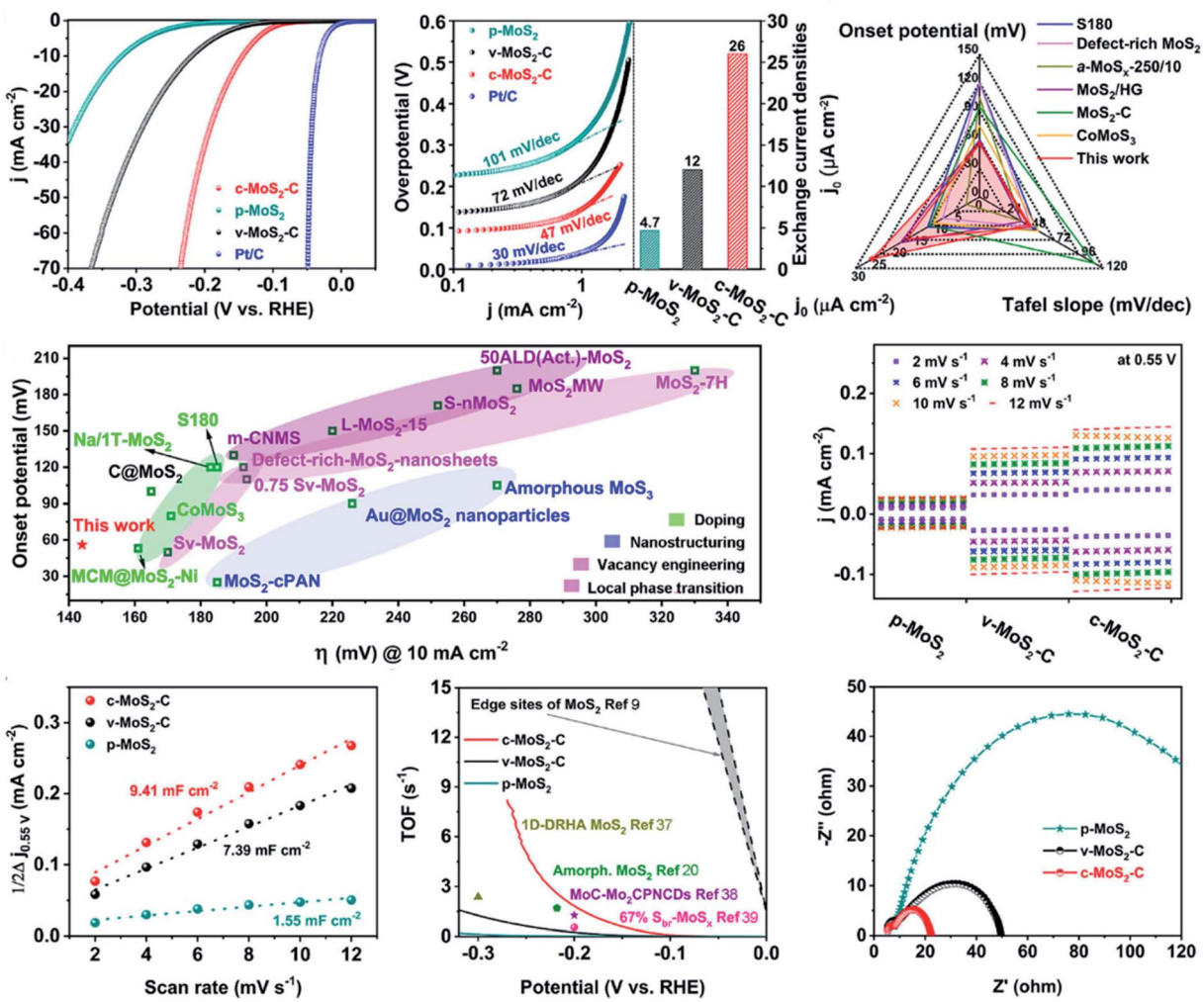

Fig. 5 The HER performance of c-MoS_2–C and the reference samples. Reproduced with permission from ref. 168, Copyright 2021 American Chemical Society.

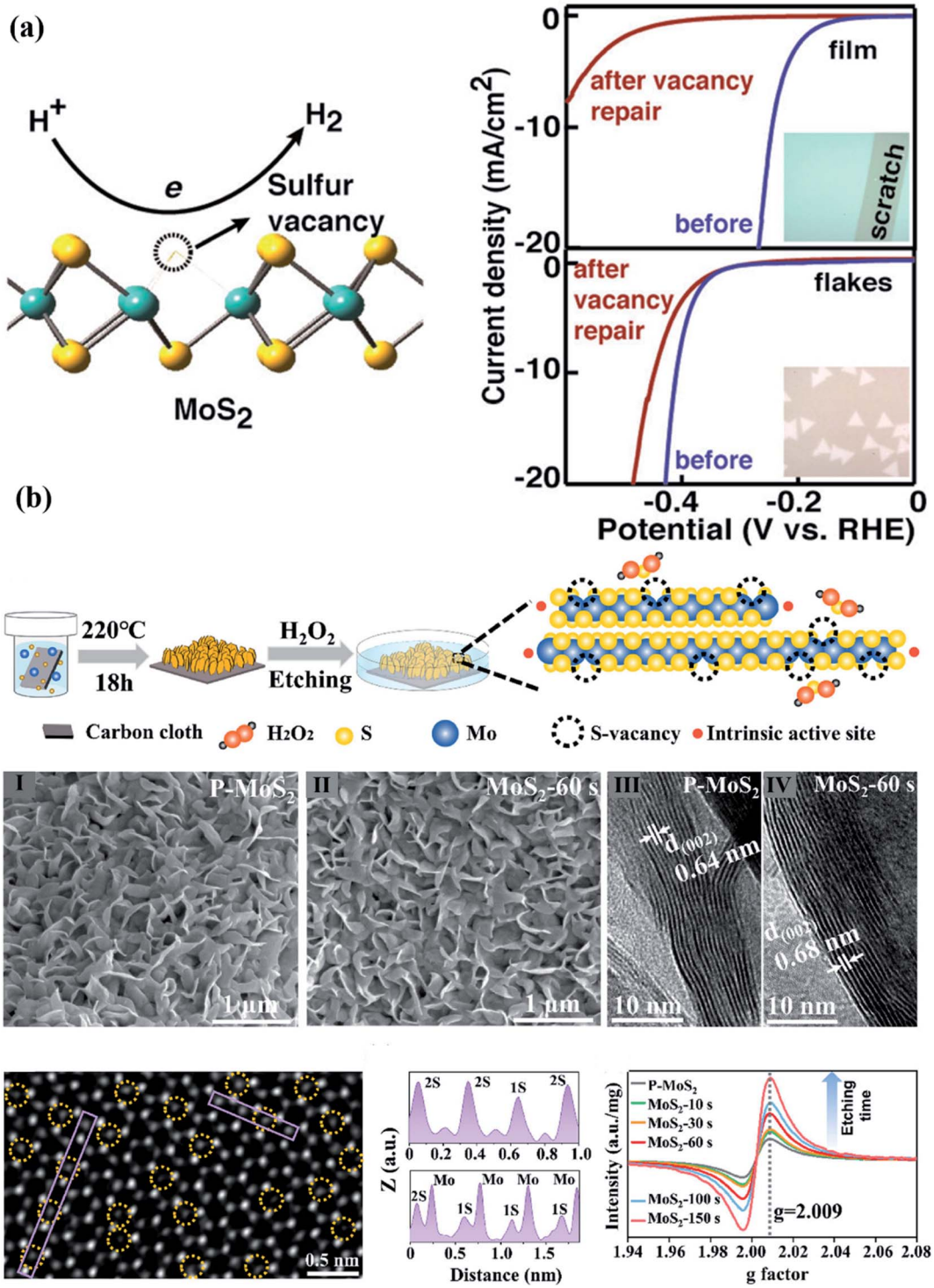

Fig. 6 (a) Schematic illustration for HER activity of MoS_2 with an S vacancy. Reproduced with permission from ref. 74, Copyright 2016 American Chemical Society. (b) Schematic of the chemical etching process to introduce single S-vacancies.

converted to the corresponding S-vacancy concentration. The electrochemical results are shown in Fig. 7(b) indicate that MoS_2 with 12.11% S-vacancy exhibited the best HER performance and the ratio of S-vacancy was very close to the theoretically predicted optimal value of 12.50%. Furthermore, the superiority of single S-vacancies over agglomerate S-vacancies was found to originate from more effective engineering of the surface electronic structure. The synergistic modulation of catalytic performance from both vacancy concentration and distribution broadens the vacancy design field and can be further extended to other types of TMDs and for other catalytic reactions.

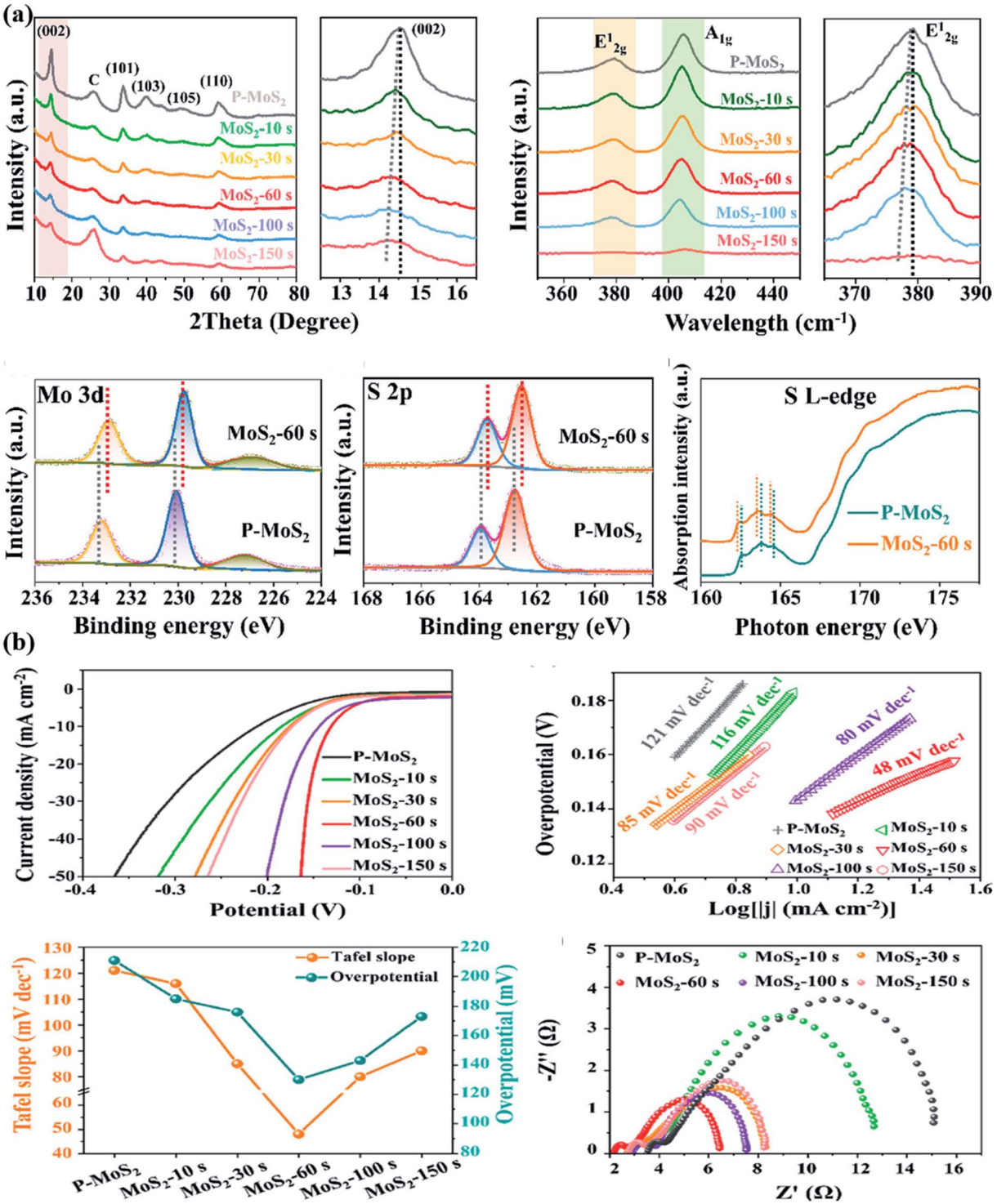

Fig. 7 (a) XRD patterns with magnified regions and Raman spectra with magnified regions of P-MoS_2 and MoS_{2-x}. High-resolution Mo 3d XPS spectrum, high-resolution S 2p XPS spectrum, and S L-edge XANES spectra of P-MoS_2 and MoS_2-60s. (b) Electrochemical HER performance of P-MoS_2 and MoS_{2-x}. Reproduced with permission from ref. 169, Copyright 2020 American Chemical Society.

Forming pits on MoS_2 monolayers has been found to be desirable for promoting HER performance. Park *et al.*[170] investigated the effect of adventitious C on the pit formation in the MoS_2 layers. They used an aperture type *in situ* ETEM to study the reaction between MoS_2 monolayers and O_2. The HER activity of MoS_2 was enhanced in the presence of pits, which can be ascribed to the increase of active edge sites (Fig. 8(b)). They also conducted DFT calculations and found that the presence of C nanoparticles on monolayer MoS_2 was favorable for progressive oxidation (Fig. 8(a)).

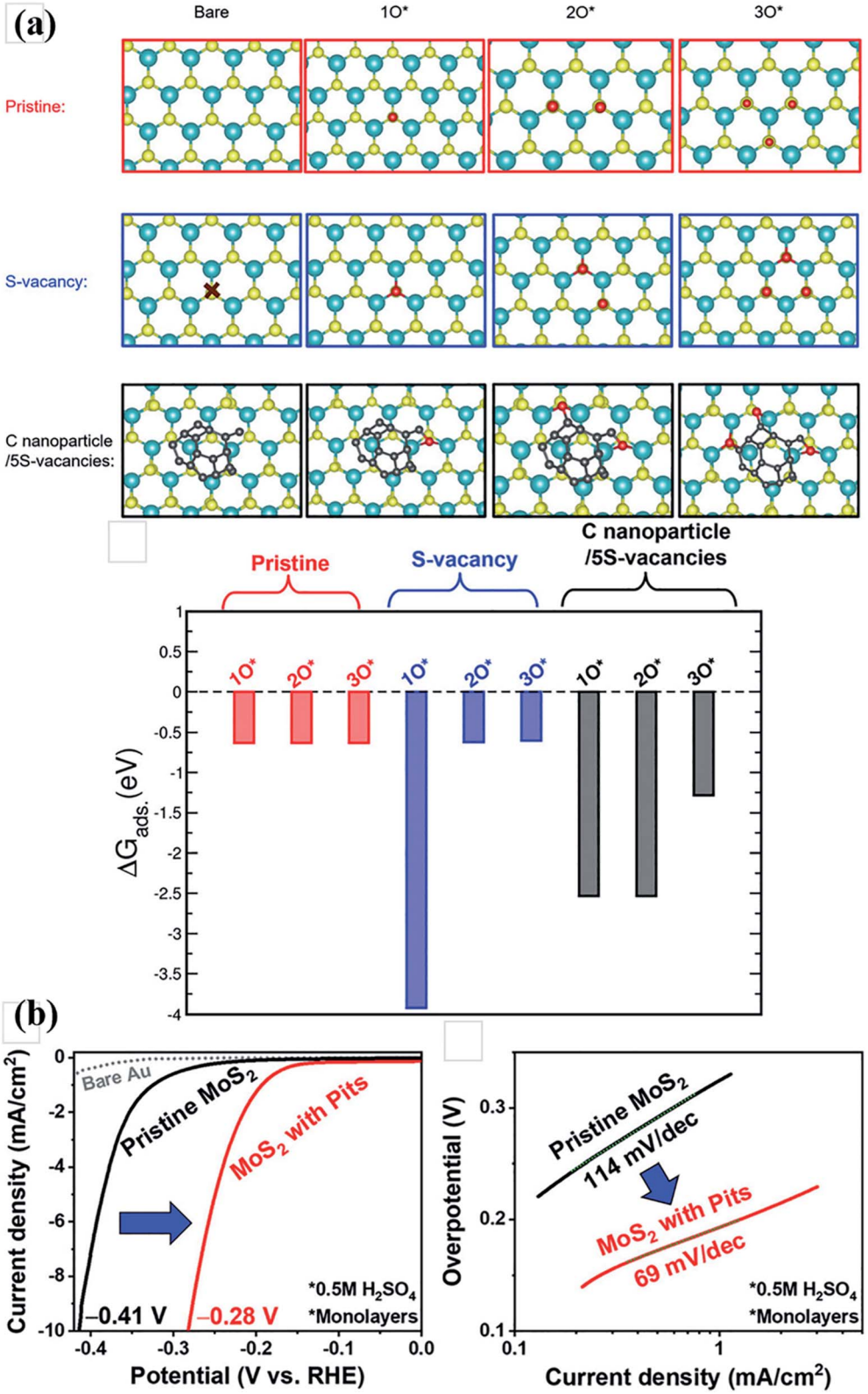

Fig. 8 (a) DFT calculation of adsorption energies of three sequential O atoms, for three different model structures. (b) Comparisons of HER activity between the pristine monolayer MoS_2 and monolayer MoS_2 with pits. Reproduced from ref. 170, Copyright 2020 John Wiley and Sons.

Although the existence of defects can significantly improve the HER performance of MoS_2, the key is the ability to detect the existence of defects. Thus, we need to study the relationship between defect types and electronic modes. Up till now, the existence of defects was observed indirectly because the concentration of defects is typically very low. One of the

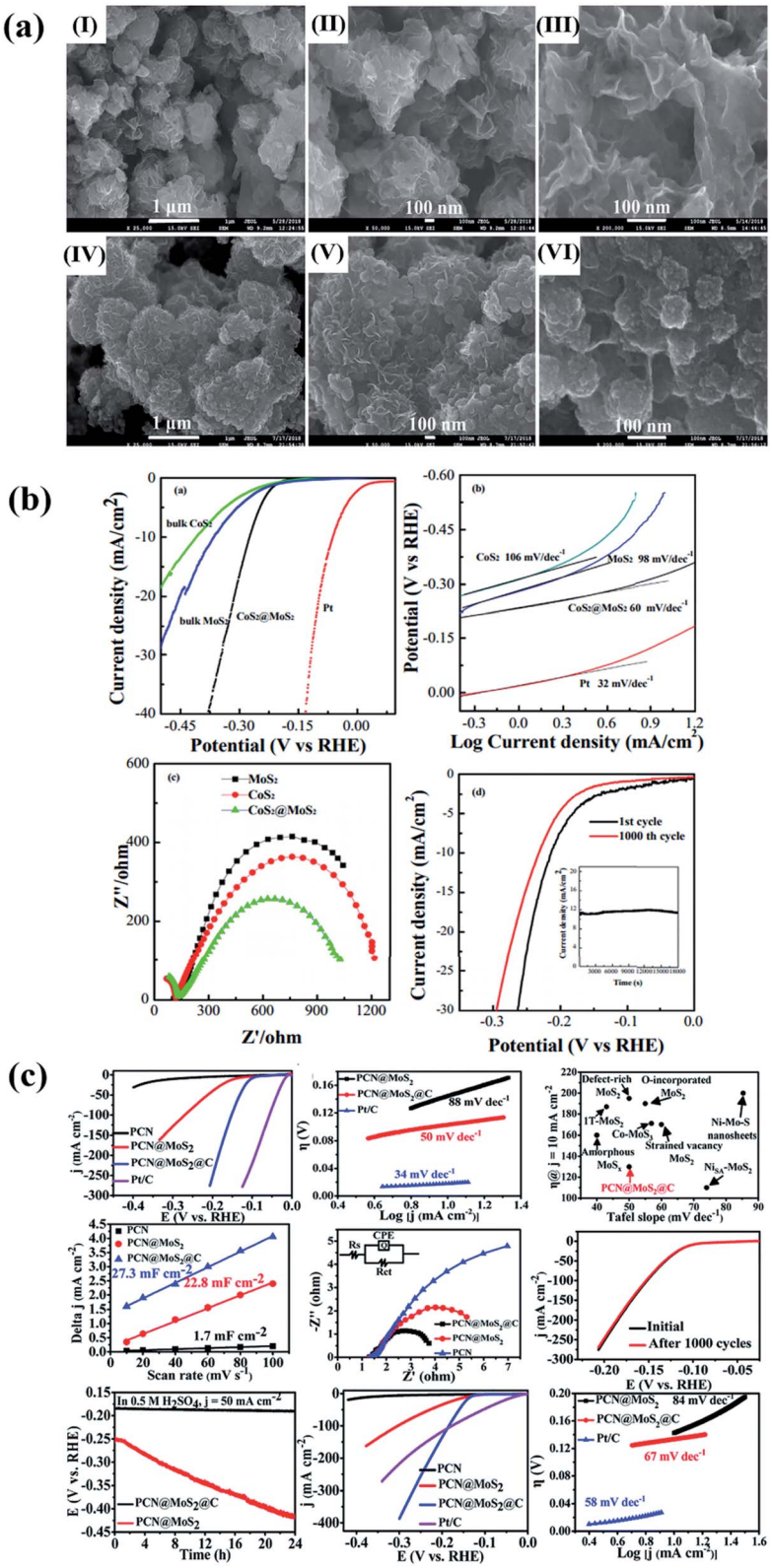

Fig. 9 (a) SEM images of bulk MoS_2 and CoS_2@MoS_2 nanoparticles. (b) HER performance of CoS_2@MoS_2. Reproduced with permission from ref. 182, Copyright 2020 Elsevier B.V. (c) The HER performance of PCN, PCN@MoS_2, PCN@MoS_2@C and Pt/C. Reproduced with permission from ref. 183, Copyright 2020 the Royal Society of Chemistry.

detecting methods is Raman spectroscopy, which can effectively detect edge defects and show distinct electronic structure. The vital task of defect engineering is to enhance the electrochemical activity of the MoS_2 basal plane.

4.2. Formation of heterostructure

The construction of heterostructured composites is an effective way to enhance the activity of MoS_2.[171–181] Wei *et al.*[182] synthesized core–shell structured CoS_2@MoS_2 by a hydrothermal method. As shown in Fig. 9(a), the CoS_2@MoS_2 nanoparticles had a uniform size distribution, ranging from 20–30 nm. The HER performance of CoS_2@MoS_2 in Fig. 9(b) shows that the overpotential of HER was only 276 mV and the Tafel slope was 60 mV dec^{-1}. Mei *et al.*[183] constructed a PCN@MoS_2@C sandwich-like heterostructure by a facile hydrothermal method. The PCN@MoS_2@C exhibited excellent HER performance within a wide pH range (Fig. 9(c)).

Constructing heterostructures with multiple electrocatalytically active components simultaneously to improve HER performance is regarded as an effective strategy. He *et al.*[184] synthesized CoS_2/SnO_2@MoS_2 (denoted as CSM) nanotubes by a fast template-engaged hydrothermal treatment. The SEM and TEM images of the obtained CSM are shown in Fig. 10(a) and (b). These images revealed a porous structure, which enlarged the surface area of the material and boosted the mass transport process, leading to excellent HER performance (Fig. 10(c)). Huang *et al.*[185] designed an exfoliated few-layer $FePS_3$ decorated with vertical MoS_2 nanosheets through a facile hydrothermal reaction. The synergistic effect between the $FePS_3$ and MoS_2 led to excellent HER performance. This effect can regulate the electronic structure and improve the electron conductivity. As

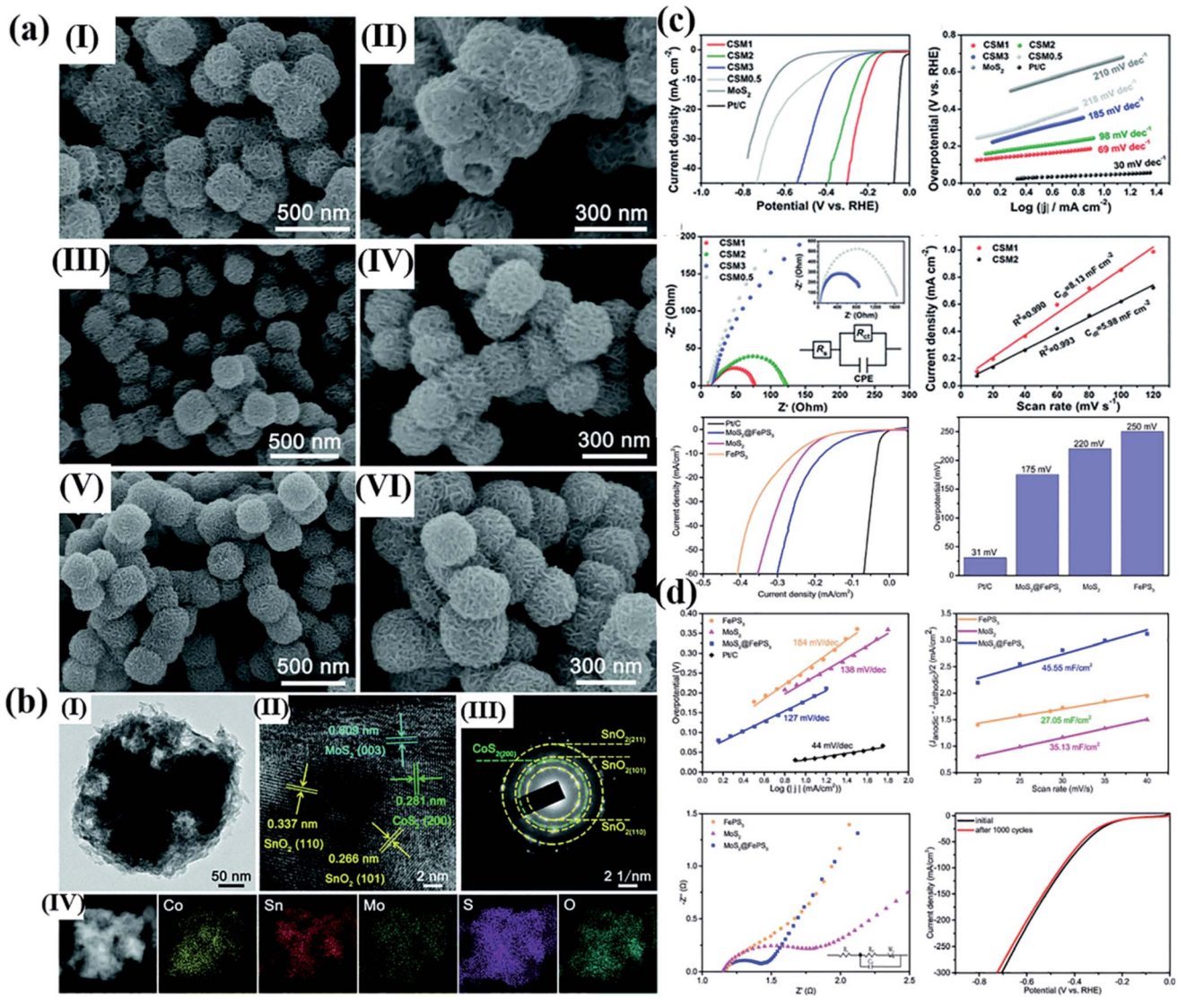

Fig. 10 (a) FESEM images of CSM1 nanocubes, CSM2 nanocubes and CSM3 nanocubes (b) TEM image, HRTEM image, the corresponding SAED pattern and TEM-EDX elemental mapping images of CSM1 nanocubes, respectively. (c) HER performance of CSM*y* ($y = 0.5, 1, 2, 3$), MoS_2 and Pt/C. Reproduced with permission from ref. 184, Copyright 2020 the Partner Organisations. (d) HER performance of $FePS_3$, MoS_2 MoS_2@$FePS_3$ and 20 wt% Pt/C. Reproduced with permission from ref. 185, Copyright 2020 Elsevier B.V.

shown in Fig. 10(d). The overpotentials of FeS_3@MoS_2 were 175 mV and 168 mV in alkaline and acidic media, respectively. Furthermore, the heterostructure could prevent agglomeration during electrocatalytic cycling, which led to high stability.

Tahira *et al.*[186] reported a stable electrocatalyst composed of TiO_2 nanorods decorated with MoS_2 nanosheets by a two-step hydrothermal method. This electrocatalyst showed an enhanced HER performance compared with bulk MoS_2 (Fig. 11(a)). Cao *et al.*[187] prepared cobalt molybdenum nitride with a nanoscale morphology using a two-step solid-state reaction. This compound did not belong to any layered structural family prepared for HER; however, it exhibited HER activity comparable to MoS_2 (Fig. 11(b)).

Theoretically, heterostructure engineering of MoS_2 with graphene is an effective and facile method and the enhanced catalytic performance can be attributed to two factors. First, the induced graphene substrate prevents the agglomeration of MoS_2 nanosheets; thus, creating sufficient edge sites for HER. Second, the excellent electronic conductivity of graphene encourages rapid electron transfer, which is beneficial for the absorption of the H atom and reduces the Gibbs free energy. Furthermore, the heterojunction of the MoS_2@graphene hybrid provides new chemical properties and may be beneficial for an enhanced HER performance. Wang *et al.*[189] constructed a MoS_2@rGO hybrid catalyst by growing MoS_2 arrays on the rGO surface *via* a one-step hydrothermal method. The MoS_2@rGO presented a three-dimensional flower-like morphology, with plentiful active edge sites exposed, which contributed to good HER performance. Yan *et al.*[190] reported a bottom-up method for the large-scale synthesis of 3D hybrid architectures constructed from graphene, MoS_2 and graphitic carbon nitride nanosheets by self-assembly. Due to the distinct architectural features such as 3D interconnected porous networks and low charge-transfer resistance, the MoS_2-CN/G exhibited superior HER performance with low overpotential, small Tafel slope and long-term durability. Wu *et al.*[191] designed MoS_2/MoN heterostructures with tuned components and the catalyst showed excellent HER performance in acid and alkaline electrocatalyst. DFT calculations suggested that the MoS_2/MoN interface could optimize the H atom adsorption kinetic energy, accelerating the HER process. Liu *et al.*[192] reported a hierarchical ZnS@C@MoS_2 core–shell nanostructure in a bottom-up strategy combined with a selective etching method. The co-existence of ZnS and porous carbon shell not only improved the electrical conductivity but also separated and loaded the MoS_2 nanosheets, which effectively exposed active edge sites. This catalyst showed an excellent HER performance with an overpotential of 118 mV and a Tafel slope of 55.4 mV dec^{-1}. Li *et al.*[193] reported a 1T-MoS_2/CoS_2 heterostructure *via* a self-sacrificing template method. In this work, they compared the cohesive energy of in-

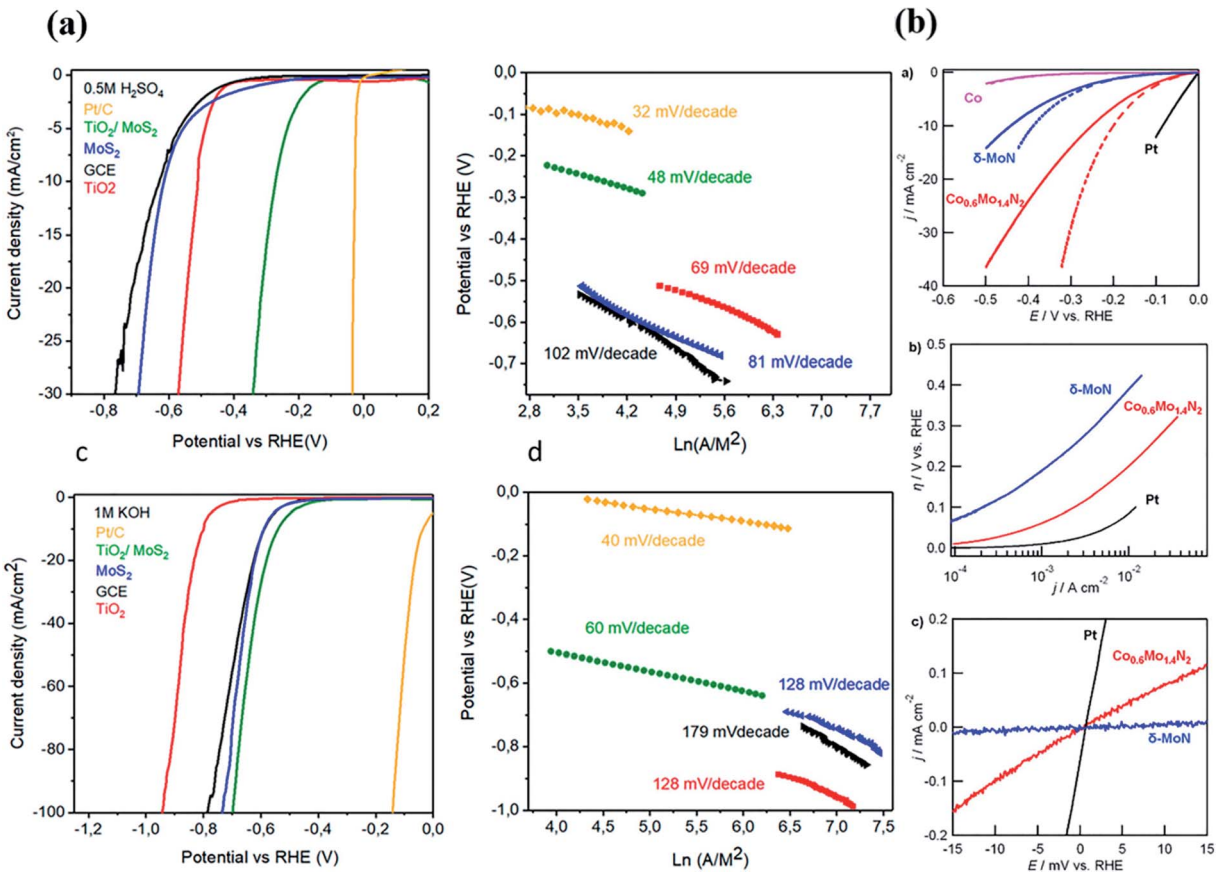

Fig. 11 (a) HER performance of TiO_2/MoS_2, TiO_2, MoS_2, Pt/C. Reproduced with permission from ref. 188, Copyright 2019 American Chemical Society. (b) HER performance of $Co_{0.6}Mo_{1.4}N_2$. Reproduced with permission from ref. 187, Copyright 2013 American Chemical Society.

plane heterostructure and out-plane heterostructure by DFT calculation and revealed that the cohesive energy of in-plane heterostructure (−5.1 eV) is much lower than that of out-plane (−4.5 eV), which demonstrated that the in-plane heterostructure is thermodynamically more stable.

4.3. Heteroatom-doping method

4.3.1. Metal-doping method. Metal doping is an effective method to promote the HER activity of MoS_2. Transition metals (Fe, Co, Ni, *etc.*) can significantly enhance the conductivity of MoS_2, and modulate the electronic structure of MoS_2. Co doping can enhance the conductivity of MoS_2, which can decrease the H atom adsorption energy of MoS_2 for HER, and also add new active catalytic sites for HER.

Xiong *et al.*[194] reported Co-doped MoS_2 nanosheets *via* a facile one-step hydrothermal method. As shown in Fig. 12(a), the obtained Co-MoS_2 exhibited superior HER activity with an overpotential of 60 mV/90 mV at a current density of 10mA cm^{-2} for HER in 0.5 M H_2SO_4 and 1.0 M KOH, respectively. They conducted DFT calculations (Fig. 12(b)) and revealed that the ΔG_{H^*} value of pristine MoS_2 was about ~2.06 eV while the ΔG_{H^*} value decreased to −0.20 eV after Co doping, demonstrating that Co doping is an effective method for enhancing HER activity of MoS_2. They also studied the OER activity origin of Co-doped MoS_2 by recording the *ex situ* Co and Mo K-edge EXAFS spectra of Co-MoS_2.

Iron is a typical nonprecious and earth-abundant element, and Fe-containing materials are more effective in adsorbing hydroxyl, which leads to its unique conductivity to water splitting.[13] Previous studies[195,196] have verified these observations through XPS characterizations. Xue *et al.*[197] synthesized a series of Fe-doped MoS_2 nanomaterials *via* a facile one-pot solvothermal method. The Fe-MoS_2 displayed high cycling stability and high HER activity with a small overpotential of 173 mV at a current density of 10 mA cm^{-2} (Fig. 12(c)). As shown in Fig. 12(d), the XPS full spectrum confirmed the existence of Fe, S, Mo and O.

Ni doping has a significant impact on surface topography and valence state of Mo in MoS_2, which can accelerate the HER reaction kinetics. Wang *et al.*[198] prepared Ni-doped MoS_2 *via* a hydrothermal method. The layer number of MoS_2 can be

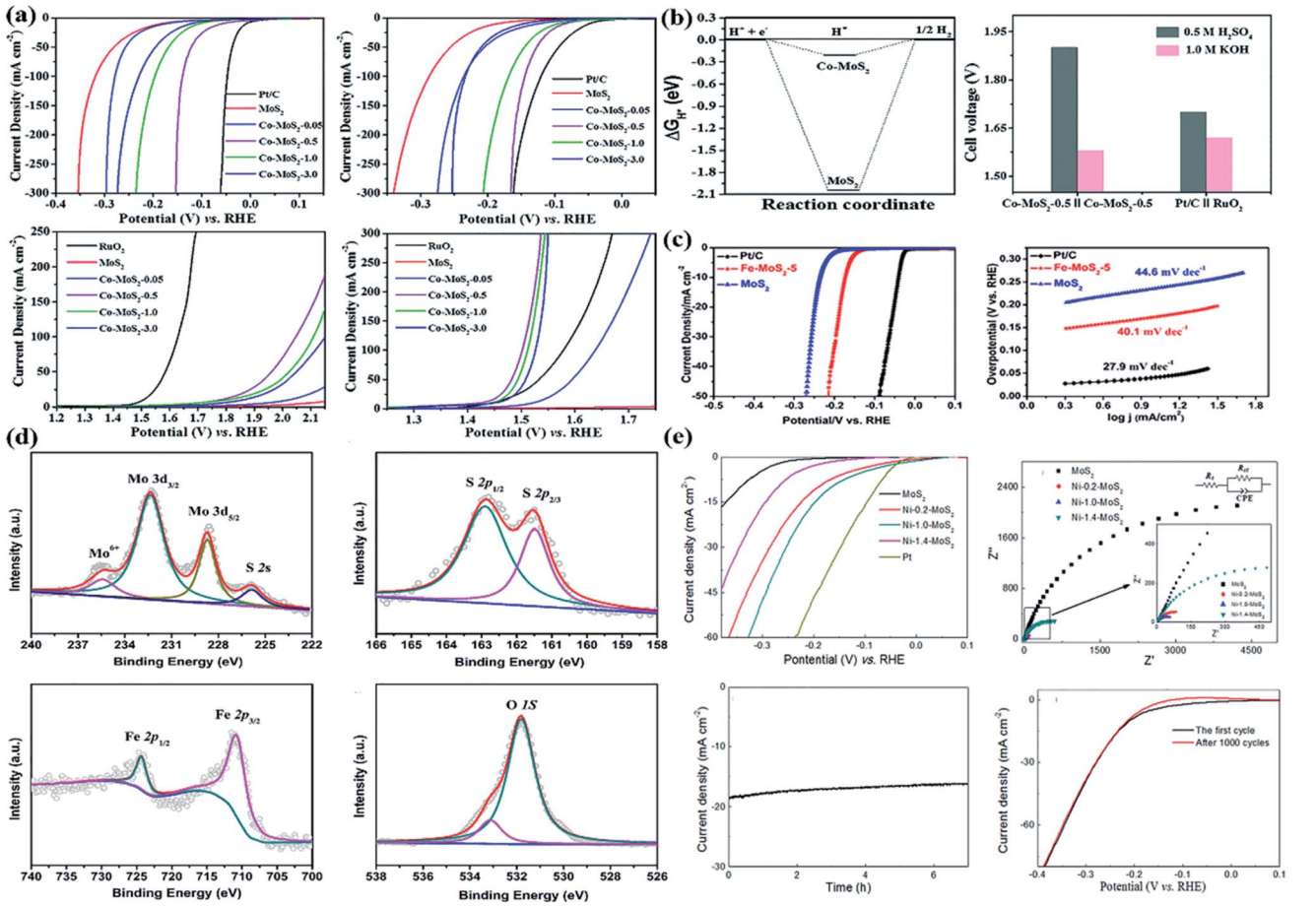

Fig. 12 (a) HER performance of Co-doped MoS_2, MoS_2 and Pt/C. (b) The H_2 adsorption free energy (ΔG_{H^*}) of MoS_2 and Co-doped MoS_2 and the cell voltage of different electrode couples in a two-electrode system in both acidic and alkaline media. Reproduced from ref. 194, Copyright 2018 The Royal Society of Chemistry. (c) HER performance of Fe-MoS_2, MoS_2 and Pt/C. (d) XPS spectra of Fe-MoS_2. Reproduced from ref. 197, Copyright 2019 American Chemical Society. (e) HER performance of Ni-MoS_2, MoS_2 and Pt/C. Reproduced from ref. 198, Copyright 2019 The Authors.

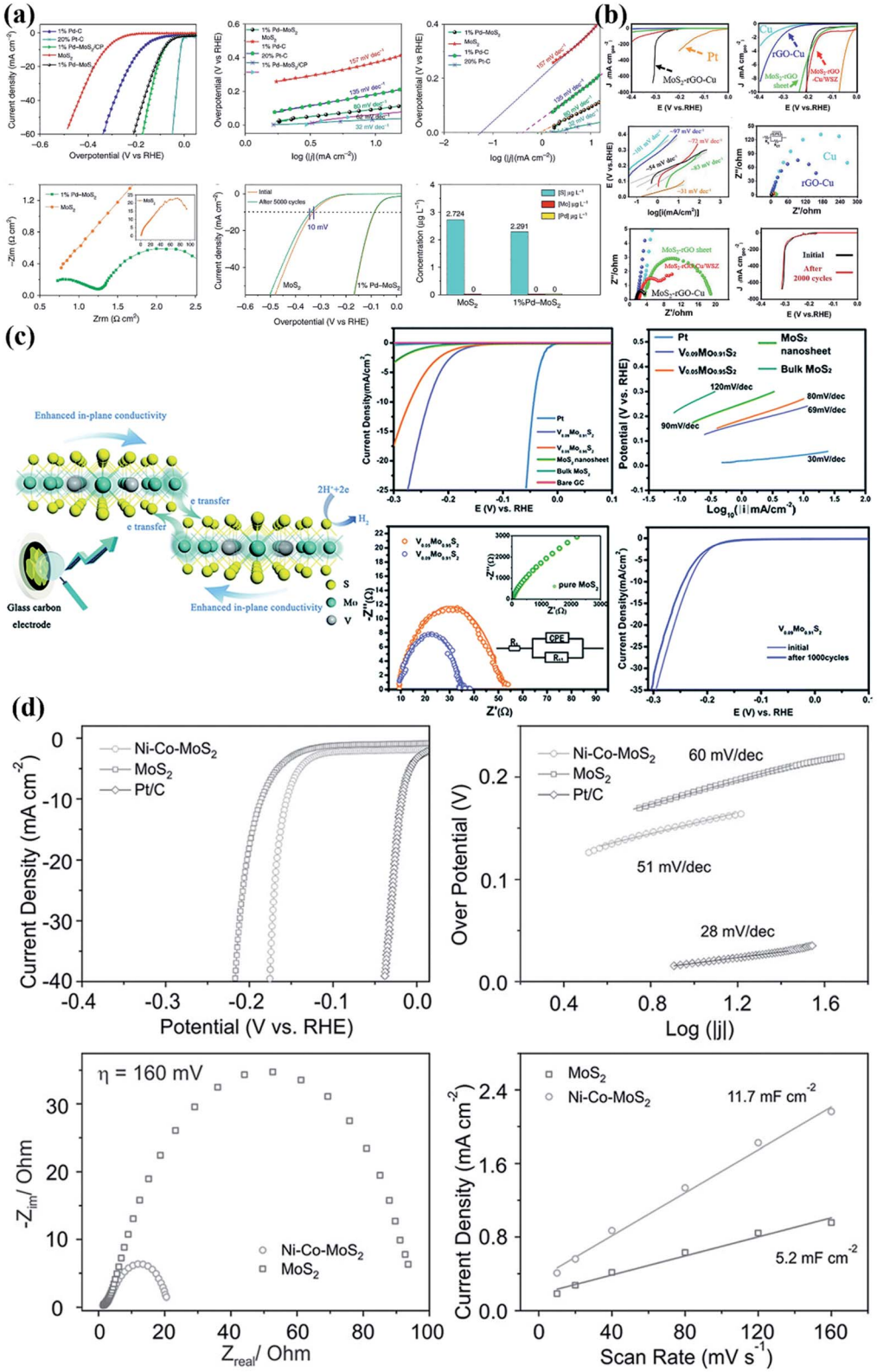

Fig. 13 (a) HER performance of Pd-MoS_2/CP and its comparison. Reproduced with permission from ref. 203, Copyright 2020 Elsevier Ltd. (b) HER performance of MoS_2–rGO–Cu and its comparison. Reproduced with permission from ref. 202, Copyright 2020 Elsevier. (c) HER performance of V-MoS_2 and its comparison. Reproduced with permission from ref. 204, Copyright 2014 The Royal Society of Chemistry. (d) HER performance of Ni–Co–MoS_2 and its comparison. Reproduced with permission from ref. 206, Copyright 2016 WILEY.

estimated by the difference in frequency between two characteristic Raman peaks. The results indicate that Ni doping decreases the vibration frequency of MoS_2 and increases the number of layers of MoS_2. Fig. 12(e) shows that the Ni-MoS_2 displayed enhanced HER performance with an overpotential of 164 mV to reach a current density of 10 mA cm^{-2} in acidic media and a small charge transfer resistance (R_{ct}) of 89 Ω.

In addition to Co, Fe, Ni doping,[198–201] some other transition metals can also promote the HER activity of MoS_2. Huang *et al.*[202] prepared a self-supporting electrode composed of Cu mesh-supported graphene and MoS_2 by electroplating zinc, followed by a hydrothermal reaction. The self-supporting catalytic electrode has the advantages of avoiding complex pretreatment of the active substance and the usage of binders. As shown in Fig. 13(b), the MoS_2–rGO–Cu exhibited excellent HER performance with a low Tafel slope of 54 mV dec^{-1} and a small overpotential of −300 mV at a current density of 400 mA cm^{-2}. The excellent HER performance can be ascribed to the good electron transport capability of the Cu mesh, and specifically, the self-supporting electrode can be fabricated into any desired shape, which is well maintained while the HER takes place. Luo *et al.*[203] designed Pd-doped MoS_2 *via* a spontaneous interfacial redox technique. The Pd doping converted 2H phase MoS_2 into a stabilized 1T structure. Furthermore, Pd atoms occurred at the Mo site, which simultaneously introduced an S vacancy. As shown in Fig. 13(a), the Pd-doped MoS_2 exhibited good cycling stability and excellent HER activity with an overpotential of 78 mV at a current density of 10 mA cm^{-2}. The DFT calculations demonstrated that the S atom next to the Pd sites had a low H atom adsorption energy of −0.02 eV. Sun *et al.*[204] designed a novel intralayer V-doping method to synthesize semi-metallic V-doped MoS_2 nanosheets. The introduction of V atoms regulated the intrinsic electrical properties of MoS_2, leading to an enhanced in-plane conductivity and shortened electron transfer paths. The V-doped MoS_2 showed excellent catalytic activity with an overpotential of 130 mV and a small Tafel slope (Fig. 13(c)). Zhang *et al.*[205] reported a single Ru atom-doped MoS_2 electrocatalyst for HER. As shown in Fig. 14(b) and (c), the DFT calculations revealed that the synergistic effects of the single Ru atom doping, S vacancies and phase transition of MoS_2 modulated the electronic structure of MoS_2 and significantly reduced the energy barrier of the Volmer step, leading to enhanced HER performance of Ru-MoS_2 (Fig. 14(a)). Multi-doping methods are also a promising way to enhance the HER activity of MoS_2. Yu *et al.*[206] reported a typical MOF-engaged synthetic method to prepare Ni and Co incorporated MoS_2 nano-boxes. The ultrathin nanosheets obtained exhibited enhanced electrochemical activity for HER (Fig. 13(d)). In recent years, materials with single-atom structure have been recognized as promising HER catalysts due to the maximized atom efficiency and tunable electronic properties. Ni *et al.*[207] reported that Ru-based single-atom catalysts are promising HER catalysts due to its excellent HER performance, which is comparable to commercial Pt/C catalysts. However, Ru-based single atom catalysts have problems such as large amount of Ru and unsatisfactory stability. Ge *et al.*[208] synthesized dual-metallic Ru and Ni atoms decorated MoS_2, which resolve the above problems well. The introduction of Ni has two key roles. On the one

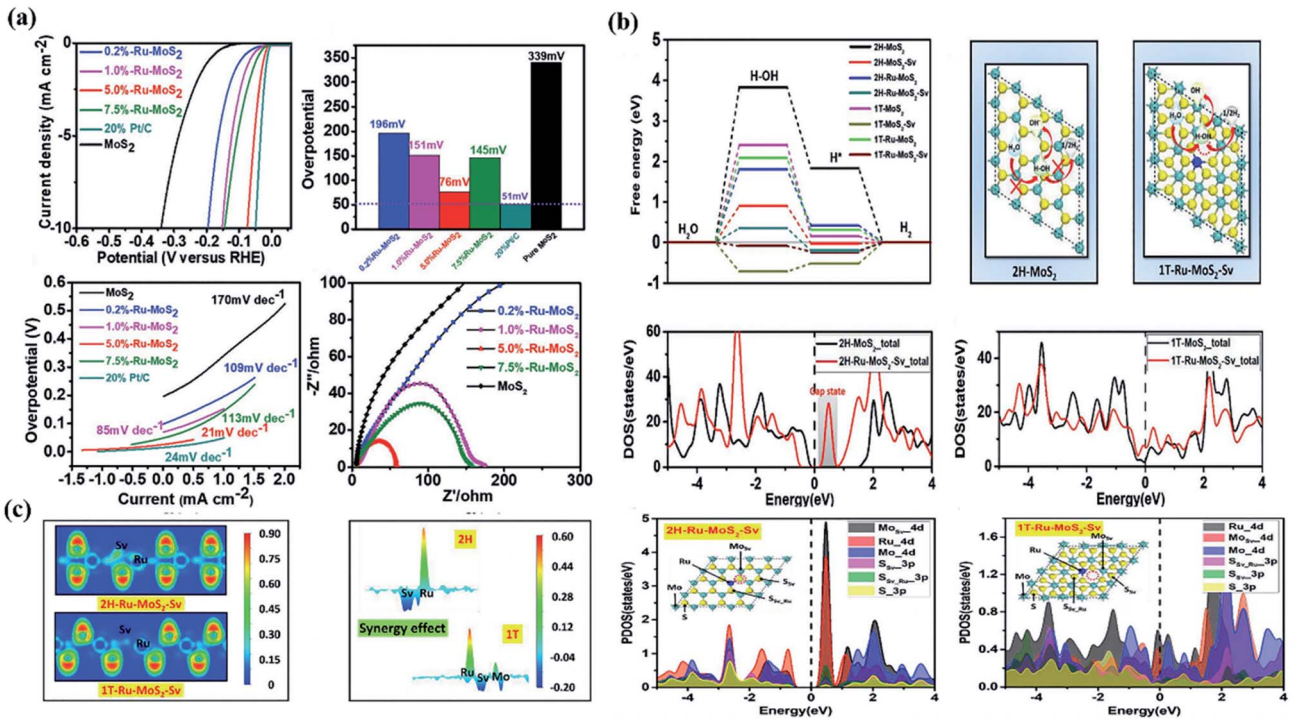

Fig. 14 (a) HER performance of Ru–MoS_2 and its comparison. (b) Free energy diagrams of the different MoS_2 model catalysts under alkaline solution. (c) Contour maps of the electron localization function (ELF) in 2H/1T-Ru-MoS_2-Sv. Reproduced with permission from ref. 205, Copyright 2019 WILEY.

hand, the introduction of highly electronegative heteroatom Ni could regulate the electronic structure of Ru and optimize the H* adsorption during the water splitting process, thus vastly enhancing the HER property. On the other hand, the incorporation of highly electronegative heteroatom Ni in the substrate exposes abundant active sites and improves electron transfer of the catalyst, and further anchors the single atom Ru and reduces the consumption of precious metal Ru atoms.

4.3.2. Nonmetal-doping method. Nonmetal doping can enhance the electrocatalytic activity of MoS_2. Wang *et al.*[209] synthesized amorphous P-doped MoS_2 nanoparticles hydrothermally. The P-doping promoted the amorphization of MoS_2; thus, affecting the HER performance of MoS_2. Deng *et al.*[210] prepared O-doped MoS_2 *via* an electrochemical anodic activation method. The HER activity of O-doped MoS_2 significantly improved at an overpotential of 50 mV, at a current density of 1 mA cm^{-2} (Fig. 15(a)). As shown in Fig. 15(b), the XPS images confirmed the strong electron interactions after O doping, which indicated the existence of Mo–O bonds and demonstrated that the O doping was successful. Liu *et al.*[211] reported O and P dual-doped MoS_2 nanosheets, which have a porous structure and conductive network *via* a one-pot hydrothermal approach. As shown in Fig. 15(c), the O, P multi-doped MoS_2 showed superior electrocatalytic performances compared with O-doped MoS_2 nanosheets. Wang *et al.*[212] prepared MoS_2 decorated Ni–Fe–N-doped carbon nanotubes *via* a hydrothermal method. According to the SEM results shown in Fig. 15(d), the catalysts were hierarchically structured. Due to the synergistic effect of the NiFe alloy and N-doped carbon nanotubes, the catalysts exhibited excellent HER performance with a cell voltage of 1.6 V at a current density of 10 mA cm^{-2}. Tian *et al.*[213] synthesized N, P dual-doped MoS_2 on hollow carbon spheres by a template and hydrothermal process. The synergistic effect of N, P dual-doped carbon and MoS_2 led to the enhanced electrocatalytic performance of MoS_2 with an overpotential of 147 mV, at a current density of 10 mA cm^{-2} and Tafel slope of 72 mV dec^{-1}. As shown in Fig. 15(e), the XPS spectra confirmed the co-existence of N and P atoms.

Metal-doping and nonmental-doping can be synergistically used to improve the HER performance of MoS_2. Meng *et al.*[214] reported a 3D mesoporous hybrid structure of Co-doped MoS_2 and graphene. The Co-doping enhanced the intrinsic

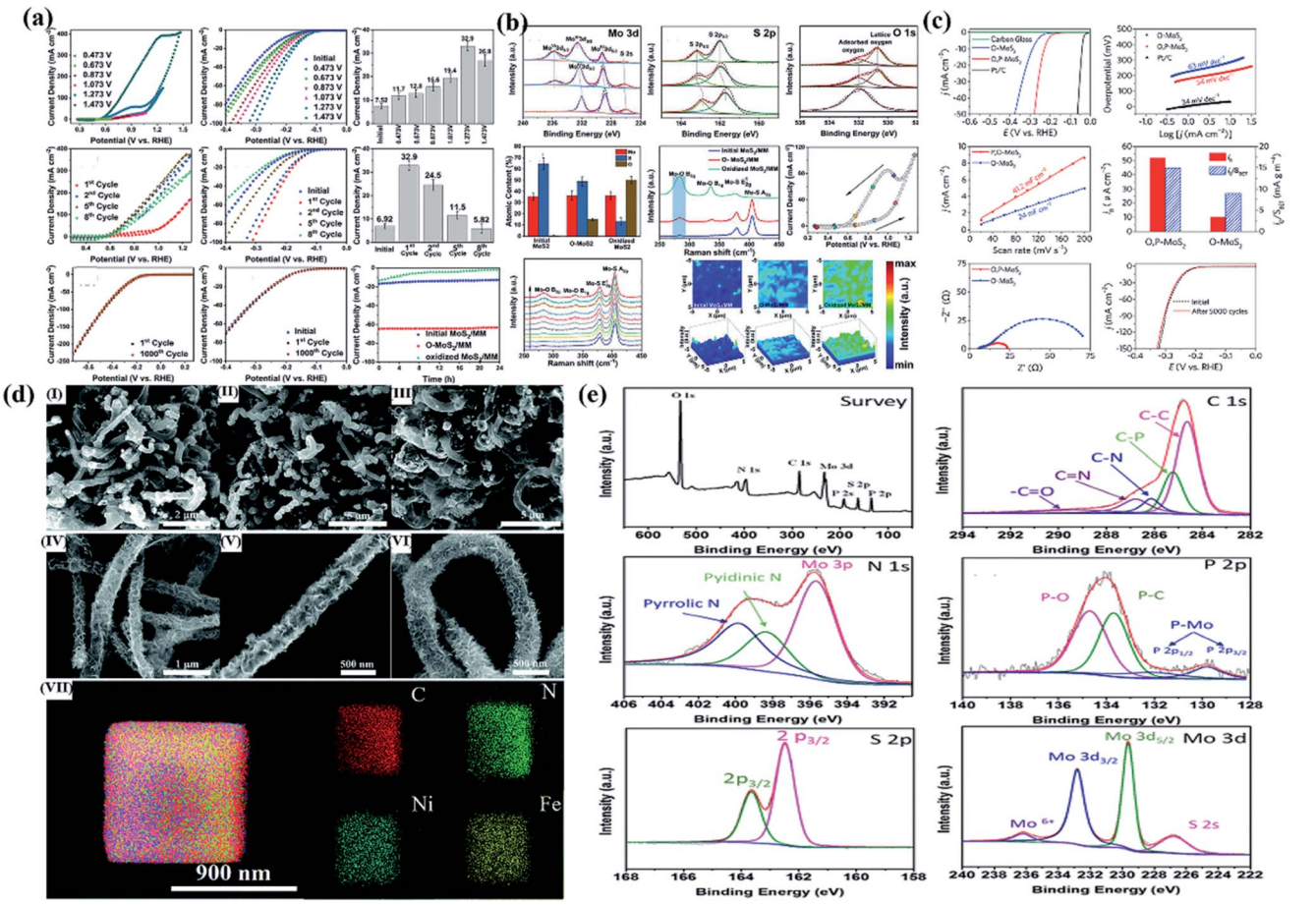

Fig. 15 (a) HER performance of O-doped MoS_2. (b) Mo 3d XPS spectra of O, P-MoS_2 ($R = 10\%$) and O-MoS_2. Reproduced with permission from ref. 210, Copyright Elsevier Ltd. (c) HER performance of O, P dual-doped MoS_2 and its comparison. Reproduced with permission from ref. 211, Copyright 2019 WILEY. (d) SEM images and elemental mapping of NiFe–NCNT–MoS_2. Reproduced with permission from ref. 212, Copyright 2019 The Royal Society of Chemistry. (e) XPS survey spectra and high-resolution scans of B, C 1s, C, N 1s, D, P 2p, E, S 2p, and F, Mo 3d electrons of the P-MoS_2@NCs-2. Reproduced with permission from ref. 213, Copyright 2021 John Wiley& Sons Ltd.

electrocatalytic activity of the in-plane S sites. The graphene network was found to be electronically conductive and robust, which improved the conductivity of electrons and enhanced the stability of the hybrid structure. The catalysts showed good cycling stability and an excellent HER performance, with an overpotential of 143 mV at a current density of 10 mA cm^{-2}. Wu *et al.*[215] designed Co, Se dual-doped electrocatalysts *via* a solvothermal and post-low-temperature selenylation process. Due to the abundance of interfaces, the electrocatalysts exhibited excellent HER performance, with a low overpotential of 58 mV at a current density of 10 mA cm^{-2} and a small Tafel slope of 84 mV dec^{-1}. Sun *et al.*[216] reported plasma-induced N, Pt-doping and phase modulation of MoS_2 nanosheets. The synergetic doping of N and Pt heteroatoms regulates the electronic and coordinated structures of MoS_2 and further facilitates water adsorption and dissociation during the HER. Notably, this plasma bombardment method is highly feasible for the large-area fabrication of MoS_2-derived HER active electrodes.

4.4. Theoretical study of the HER

The studies of electronic structures of MoS_2 offer theoretical guidance for designing efficient catalysts. For MoS_2, a typical 2D material, the theoretical calculation of the basal plane positions, Mo edge and S edge is quite significant. Furthermore, it is also beneficial to investigate the adsorption energy of intermediates. Jacob *et al.*[217] proposed an H-binding mechanism for S atoms in the basal plane of MoS_2. This model was tested and verified by DFT calculations; herein, the energy barrier can be

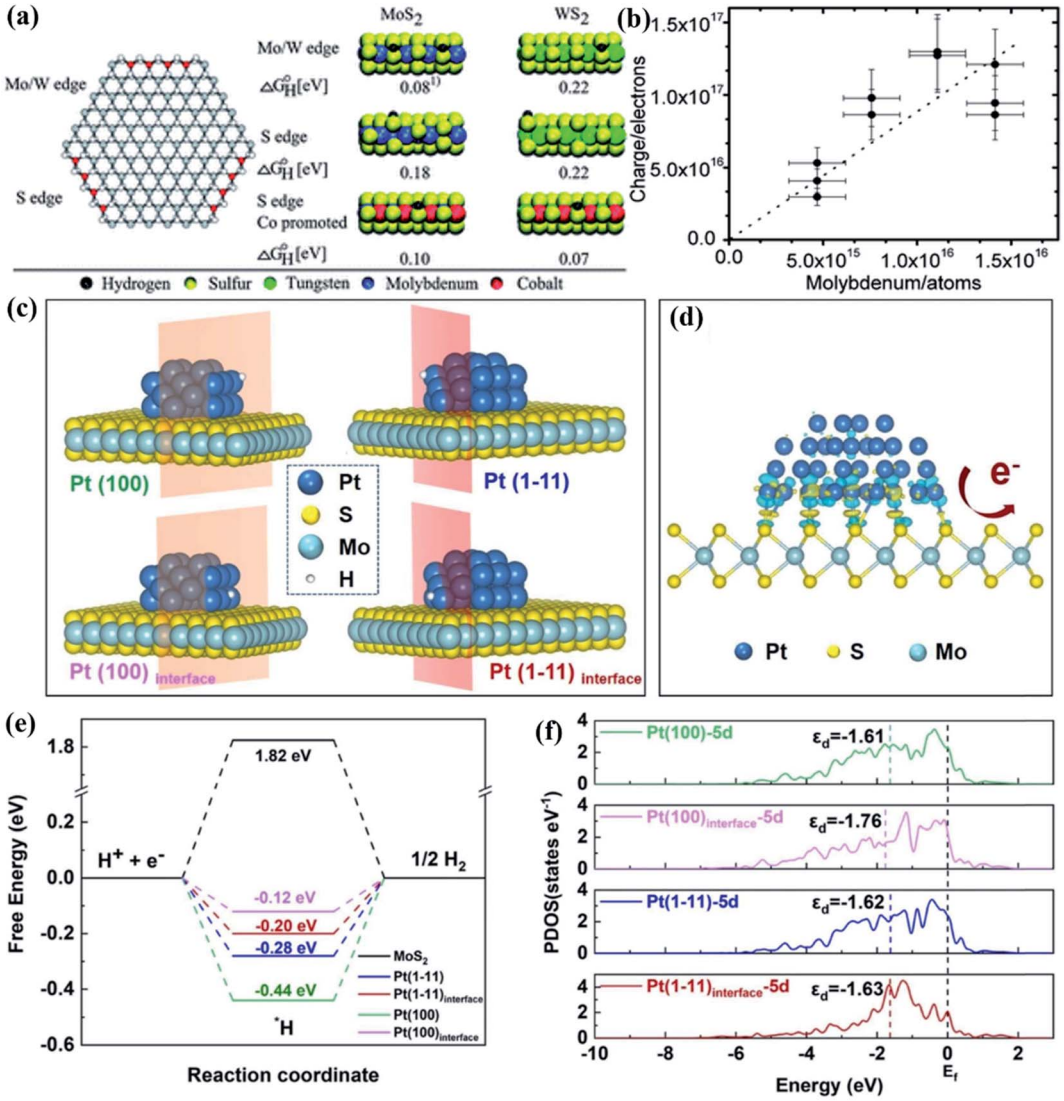

Fig. 16 (a) Left: ball model of a Mo/WS_2 particle exposing both S-edge and Mo/W-edge. Right: differential free energies of H atom adsorption. (b) The charge of the irreversible oxidation peak as a function of the amount of Mo used during the synthesis of MoS_2 Reproduced with permission from ref. 217, Copyright 2008 The Royal Society of Chemistry. (c) The side views of the atomic model of Pt truncated octahedron loaded on MoS_2. (d) Charge-density difference for Pt-MoS_2. The decrease of electron density is shown in yellow, and increase is shown in blue. (e) The adsorption Gibbs free energy of hydrogen on the above Pt positions and the surface for MoS_2. (f) The partial density of states (PDOS) of Pt atoms on the above positions. Reproduced with permission from ref. 218, Copyright 2022 Elsevier.

tuned by introducing metal dopants and defects. Their study revealed the electronic structure mechanism which tends to influence the basal plane S atoms activation (Fig. 16(a) and (b)). Xian *et al.*[218] synthesized the monodispersed single-crystal Pt nanoparticles decorated on 2H phase MoS_2 nanosheets *via* a wet chemical method. They construct the atomic model of Pt truncated octahedron loaded on MoS_2, and choose four Pt sites (Fig. 16(c)). The charge-density difference is showed in Fig. 16(d), indicating the variations of the charge distributions for Pt and S at the interface of Pt-MoS_2 atomic model from those for pure Pt and S. The results reveal that the Pt–S bonds are formed. Then, they calculate the free energy of adsorbed atomic hydrogen (ΔG_{H^*}), including MoS_2 (001), Pt (100), Pt (100) $_{interface}$, Pt (1–11) and Pt (1–11) $_{interface}$ (Fig. 16(e)). The results indicate that the Pt (100) $_{interface}$ owns the smallest ΔG_{H^*} as well as the best HER activity. Further, they found that with the studied Pt atoms changing to the interface, the D-band center move away from the Fermi level (Fig. 14(f)), indicating the decrease of ΔG_{H^*}, which confirms the superiority for Pt (100) $_{interface}$ in HER performance. In published DFT studies, the electronic structures of MoS_2-based materials are usually computed by VASP and the electron–ion interactions are described by the projector-augmented wave method. All calculations are typically implemented with PBE exchange–correlation functional on periodically repeated slabs. The details of the molecular model-building, HER mechanism and free-energy calculations are provided in the relevant ref. 219–222.

5. Conclusions and outlook

With the depletion of traditional fossil energy, the development of green energy such as hydrogen energy has become urgent. Electrocatalytic water splitting to produce hydrogen offers a means to develop new energy sources. Up to now, significant progress has been made in achieving effecting hydrogen evolution reactions (HERs) using promising electrocatalysts such as transition metal sulfides (TMDs), transition metal carbides (TMCs), transition metal phosphides (TMPs) and transition metal nitrides (TMNs). As a typical electrocatalyst, MoS_2 has been widely studied and much progress has been made. In this review, we summarize the synthetic methods of MoS_2 and the effective strategies adopted to optimize the HER performance of MoS_2. The introduction of defects significantly enhanced the HER activity of the MoS_2-based materials, which was also verified theoretically. The formation of heterostructures is another effective way to enhance the HER activity of MoS_2, which can modulate the electronic structure. Furthermore, doping metal atoms (Fe, Co, Ni, Cu, Mn, V, Ru *etc.*) or nonmetal atoms (C, N, F, P, S, Se *etc.*) into MoS_2 can also improve its electrocatalytic HER performance.

However, there are still some challenges for the commercial application of MoS_2-based materials. Firstly, even though ultrathin MoS_2-based materials can be synthesized by CVD and hydrothermal methods, the large-scale production of MoS_2 is still a challenge. Secondly, the standards for evaluating electrocatalytic stability have not yet been developed. Thirdly, while DFT calculations can provide a detailed theoretical insight into the reaction mechanism of a single active center, research involving the existence of multiple active centers is still lacking. Fourthly, the catalytic influence of H_2O on the MoS_2 surface and interlayers is still not completely understood because of the difficulty to develop bifunctional electrocatalysts for all electrolytes. Lastly, vacancies, doping atoms, and heterojunctions usually have a positive effect on the electrocatalytic process. However, the reaction mechanism needs to be further explored.

While there is still a long way to go for the development of MoS_2-based electrocatalytic materials, the research interest in this area is increasing. Moreover, with the rapid development of computational tools, it is possible to make advances in many experimental areas, including MoS_2-based materials. From this point of view, we can foresee that MoS_2-based materials will be very promising for hydrogen production applications.

Conflicts of interest

The authors declare no competing financial interest.

Acknowledgements

This research was supported by National Science and Technology Major Project (Grant No. 2020YFB1506001) and Department of Science and Technology of Sichuan Province (Grant No. 2021YFG0231).

References

1 M. A. Shannon, P. W. Bohn, M. Elimelech, J. G. Georgiadis, B. J. Marinas and A. M. Mayes, *Nature*, 2008, **452**, 301–310.
2 D. Larcher and J. M. Tarascon, *Nat. Chem.*, 2015, **7**, 19–29.
3 A. Fiaz, D. Zhu and J. Sun, *Environ. Sci. Eur.*, 2021, **33**, 64–80.
4 L. Han, S. Dong and E. Wang, *Adv. Mater.*, 2016, **28**, 9266–9291.
5 I. K. Kapdan and F. Kargi, *Enzyme Microb. Technol.*, 2006, **38**, 569–582.
6 S. H. Mousavi-Avval, S. Rafiee, A. Jafari and A. Mohammadi, *J. Clean. Prod.*, 2011, **19**, 1464–1470.
7 P. Nugent, Y. Belmabkhout, S. D. Burd, A. J. Cairns, R. Luebke, K. Forrest, T. Pham, S. Ma, B. Space, L. Wojtas, M. Eddaoudi and M. J. Zaworotko, *Nature*, 2013, **495**, 80–84.
8 A. Kudo and Y. Miseki, *Chem. Soc. Rev.*, 2009, **38**, 253–278.
9 Y. Li, H. Wang, L. Xie, Y. Liang, G. Hong and H. Dai, *J. Am. Chem. Soc.*, 2011, **133**, 7296–7299.
10 Y. Liang, Y. Li, H. Wang, J. Zhou, J. Wang, T. Regier and H. Dai, *Nat. Mater.*, 2011, **10**, 780–786.
11 C. C. McCrory, S. Jung, J. C. Peters and T. F. Jaramillo, *J. Am. Chem. Soc.*, 2013, **135**, 16977–16987.
12 S. Zhao, Y. Wang, J. Dong, C.-T. He, H. Yin, P. An, K. Zhao, X. Zhang, C. Gao, L. Zhang, J. Lv, J. Wang, J. Zhang, A. M. Khattak, N. A. Khan, Z. Wei, J. Zhang, S. Liu, H. Zhao and Z. Tang, *Nat. Energy*, 2016, **1**, 184–193.
13 S. Li, J. Sun and J. Guan, *Chin. J. Catal.*, 2021, **42**, 511–556.
14 Y. Chen, Q. Zhou, G. Zhao, Z. Yu, X. Wang, S. X. Dou and W. Sun, *Adv. Funct. Mater.*, 2017, **28**, 170–176.

15 C. Liu, G. Zhang, L. Yu, J. Qu and H. Liu, *Small*, 2018, **14**, 180–188.
16 J. Deng, H. Li, J. Xiao, Y. Tu, D. Deng, H. Yang, H. Tian, J. Li, P. Ren and X. Bao, *Energy Environ. Sci.*, 2015, **8**, 1594–1601.
17 D. Y. Wang, M. Gong, H. L. Chou, C. J. Pan, H. A. Chen, Y. Wu, M. C. Lin, M. Guan, J. Yang, C. W. Chen, Y. L. Wang, B. J. Hwang, C. C. Chen and H. Dai, *J. Am. Chem. Soc.*, 2015, **137**, 1587–1592.
18 J. Deng, P. Ren, D. Deng, L. Yu, F. Yang and X. Bao, *Energy Environ. Sci.*, 2014, **7**, 1919–1923.
19 M. S. Faber, M. A. Lukowski, Q. Ding, N. S. Kaiser and S. Jin, *J. Phys. Chem. C Nanomater. Interfaces*, 2014, **118**, 21347–21356.
20 Q. Gong, L. Cheng, C. Liu, M. Zhang, Q. Feng, H. Ye, M. Zeng, L. Xie, Z. Liu and Y. Li, *ACS Catal.*, 2015, **5**, 2213–2219.
21 J. Kibsgaard, C. Tsai, K. Chan, J. D. Benck, J. K. Nørskov, F. Abild-Pedersen and T. F. Jaramillo, *Energy Environ. Sci.*, 2015, **8**, 3022–3029.
22 M. Zeng and Y. Li, *J. Mater. Chem. A*, 2015, **3**, 14942–14962.
23 Y. Tan, H. Wang, P. Liu, Y. Shen, C. Cheng, A. Hirata, T. Fujita, Z. Tang and M. Chen, *Energy Environ. Sci.*, 2016, **9**, 2257–2261.
24 A. Eftekhari, *Int. J. Hydrogen Energy*, 2017, **42**, 11053–11077.
25 Y. Jia, L. Zhang, G. Gao, H. Chen, B. Wang, J. Zhou, M. T. Soo, M. Hong, X. Yan, G. Qian, J. Zou, A. Du and X. Yao, *Adv. Mater.*, 2017, **29**, 798–805.
26 H. Sun, Z. Yan, F. Liu, W. Xu, F. Cheng and J. Chen, *Adv. Mater.*, 2020, **32**, 326–334.
27 J. Feng, F. Lv, W. Zhang, P. Li, K. Wang, C. Yang, B. Wang, Y. Yang, J. Zhou, F. Lin, G. C. Wang and S. Guo, *Adv. Mater.*, 2017, **29**, 288–296.
28 M. S. Faber and S. Jin, *Energy Environ. Sci.*, 2014, **7**, 3519–3542.
29 H. Vrubel and X. Hu, *Angew. Chem., Int. Ed.*, 2012, **51**, 12703–12706.
30 W. F. Chen, J. T. Muckerman and E. Fujita, *Chem. Commun.*, 2013, **49**, 8896–8909.
31 Z. W. Seh, K. D. Fredrickson, B. Anasori, J. Kibsgaard, A. L. Strickler, M. R. Lukatskaya, Y. Gogotsi, T. F. Jaramillo and A. Vojvodic, *ACS Energy Lett.*, 2016, **1**, 589–594.
32 X. Wang, Y. V. Kolen'ko, X. Q. Bao, K. Kovnir and L. Liu, *Angew. Chem., Int. Ed.*, 2015, **54**, 8188–8192.
33 C. Liu, L. Sun, L. Luo, W. Wang, H. Dong and Z. Chen, *ACS Appl. Mater. Interfaces*, 2021, **13**, 22646–22654.
34 X. Zhang, Z. Zhu, X. Liang, F.-X. Ma, J. Zhang, Y. Tan, Z. Pan, Y. Bo and C.-M. Lawrence Wu, *Chem. Eng. J.*, 2021, **408**, 1910–1916.
35 A. A. Koverga, E. Flórez, C. Jimenez-Orozco and J. A. Rodriguez, *Electrochim. Acta*, 2021, **368**, 351–359.
36 B. Zhang, H. Qin, Y. Pan, W. Lin, S. Xu, Q. Sun, E. Liu, F. He, L. Diao, C. He and L. Ma, *ACS Appl. Nano Mater.*, 2020, **4**, 372–380.
37 D. Kong, J. J. Cha, H. Wang, H. R. Lee and Y. Cui, *Energy Environ. Sci.*, 2013, **6**, 3553–3558.
38 J. Xie, J. Zhang, S. Li, F. Grote, X. Zhang, H. Zhang, R. Wang, Y. Lei, B. Pan and Y. Xie, *J. Am. Chem. Soc.*, 2013, **135**, 17881–17888.
39 J. Chen, X. J. Wu, L. Yin, B. Li, X. Hong, Z. Fan, B. Chen, C. Xue and H. Zhang, *Angew. Chem., Int. Ed.*, 2015, **54**, 1210–1214.
40 R. Lv, J. A. Robinson, R. E. Schaak, D. Sun, Y. Sun, T. E. Mallouk and M. Terrones, *Acc. Chem. Res.*, 2015, **48**, 56–64.
41 S. Xu, D. Li and P. Wu, *Adv. Funct. Mater.*, 2015, **25**, 1127–1136.
42 Y. Jiao, Y. Zheng, K. Davey and S.-Z. Qiao, *Nat. Energy*, 2016, **1**, 160–169.
43 Q. Lu, Y. Yu, Q. Ma, B. Chen and H. Zhang, *Adv. Mater.*, 2016, **28**, 1917–1933.
44 D. Voiry, J. Yang and M. Chhowalla, *Adv. Mater.*, 2016, **28**, 6197–6206.
45 S. P. Kaur and T. J. Dhilip Kumar, *Appl. Surf. Sci.*, 2021, **552**, 3002–3012.
46 P. Jiang, Q. Liu, Y. Liang, J. Tian, A. M. Asiri and X. Sun, *Angew. Chem., Int. Ed.*, 2014, **53**, 12855–12859.
47 Y. Shi and B. Zhang, *Chem. Soc. Rev.*, 2016, **45**, 1529–1541.
48 S. M. El-Refaei, P. A. Russo and N. Pinna, *ACS Appl. Mater. Interfaces*, 2021, **13**, 22077–22097.
49 W. Pei, X. Wang, C. Liu, D. Zhao, C. Wu, K. Wang and Q. Wang, *Electrochim. Acta*, 2021, **381**, 286–296.
50 Y. Jeung, H. Jung, D. Kim, H. Roh, C. Lim, J. W. Han and K. Yong, *J. Mater. Chem. A*, 2021, **9**, 12203–12213.
51 R. Zhang, Y. Dong, M. A. Al-Tahan, Y. Zhang, R. Wei, Y. Ma, C. Yang and J. Zhang, *J. Energy Chem.*, 2021, **60**, 85–94.
52 W. J. Yu, Z. Li, H. Zhou, Y. Chen, Y. Wang, Y. Huang and X. Duan, *Nat. Mater.*, 2013, **12**, 246–252.
53 A. S. Sethulekshmi, J. S. Jayan, S. Appukuttan and K. Joseph, *Phys. E Low-dimens. Syst. Nanostruct.*, 2021, **132**, 89–96.
54 S. Park, C. Kim, S. O. Park, N. K. Oh, U. Kim, J. Lee, J. Seo, Y. Yang, H. Y. Lim, S. K. Kwak, G. Kim and H. Park, *Adv. Mater.*, 2020, **32**, 18–29.
55 W. Chen, Z. Wang, K. V. Bets, D. X. Luong, M. Ren, M. G. Stanford, E. A. McHugh, W. A. Algozeeb, H. Guo, G. Gao, B. Deng, J. Chen, J. T. Li, W. T. Carsten, B. I. Yakobson and J. M. Tour, *ACS Nano*, 2021, **15**, 1282–1290.
56 J. Huang, X. Pan, X. Liao, M. Yan, B. Dunn, W. Luo and L. Mai, *Nanoscale*, 2020, **12**, 9246–9254.
57 H. He, X. Li, D. Huang, J. Luan, S. Liu, W. K. Pang, D. Sun, Y. Tang, W. Zhou, L. He, C. Zhang, H. Wang and Z. Guo, *ACS Nano*, 2021, **15**, 8896–8906.
58 J. Dong, X. Zhang, J. Huang, J. Hu, Z. Chen and Y. Lai, *Chem. Eng. J.*, 2021, **412**, 556–576.
59 B. Gao, Y. Zhao, X. Du, Y. Chen, B. Guan, Y. Li, Y. Li, S. Ding, H. Zhao, C. Xiao and Z. Song, *J. Mater. Chem. A*, 2021, **9**, 8394–8400.
60 N. Zhao, L. Wang, Z. Zhang and Y. Li, *ACS Appl. Mater. Interfaces*, 2019, **11**, 42014–42020.
61 X. Wang, C. Wang, S. Ci, Y. Ma, T. Liu, L. Gao, P. Qian, C. Ji and Y. Su, *J. Mater. Chem. A*, 2020, **8**, 23488–23497.

62 Y. Chen, J. Rong, Q. Tao, C. Xing, M. Lian, J. Cheng, X. Liu, J. Cao, M. Wei, S. Lv, P. Zhu, L. Yang and J. Yang, *Electrochim. Acta*, 2020, **357**, 1307–1315.
63 A. Q. Mugheri, S. Ali, G. S. Narejo, A. A. Otho, R. Lal, M. A. Abro, S. H. Memon and F. Abbasi, *Int. J. Hydrogen Energy*, 2020, **45**, 21502–21511.
64 X. Xin, Y. Song, S. Guo, Y. Zhang, B. Wang, J. Yu and X. Li, *Appl. Catal. B Environ.*, 2020, **269**, 773–780.
65 A. Jalil, Z. Zhuo, Z. Sun, F. Wu, C. Wang and X. Wu, *J. Mater. Chem. A*, 2020, **8**, 1307–1314.
66 J. Zhang, T. Wang, P. Liu, S. Liu, R. Dong, X. Zhuang, M. Chen and X. Feng, *Energy Environ. Sci.*, 2016, **9**, 2789–2793.
67 Y. Li, H. Li, K. Cao, T. Jin, X. Wang, H. Sun, J. Ning, Y. Wang and L. Jiao, *Energy Storage Mater.*, 2018, **12**, 44–53.
68 M. S. Faber, R. Dziedzic, M. A. Lukowski, N. S. Kaiser, Q. Ding and S. Jin, *J. Am. Chem. Soc.*, 2014, **136**, 10053–10061.
69 D. Voiry, R. Fullon, J. Yang, E. S. C. de Carvalho Castro, R. Kappera, I. Bozkurt, D. Kaplan, M. J. Lagos, P. E. Batson, G. Gupta, A. D. Mohite, L. Dong, D. Er, V. B. Shenoy, T. Asefa and M. Chhowalla, *Nat. Mater.*, 2016, **15**, 1003–1009.
70 T. Zhang, M.-Y. Wu, D.-Y. Yan, J. Mao, H. Liu, W.-B. Hu, X.-W. Du, T. Ling and S.-Z. Qiao, *Nano Energy*, 2018, **43**, 103–109.
71 Y. Li, J. Yin, L. An, M. Lu, K. Sun, Y. Q. Zhao, D. Gao, F. Cheng and P. Xi, *Small*, 2018, **14**, 70–78.
72 S. Peng, F. Gong, L. Li, D. Yu, D. Ji, T. Zhang, Z. Hu, Z. Zhang, S. Chou, Y. Du and S. Ramakrishna, *J. Am. Chem. Soc.*, 2018, **140**, 13644–13653.
73 Y. Da, J. Liu, L. Zhou, X. Zhu, X. Chen and L. Fu, *Adv. Mater.*, 2019, **31**, 93–99.
74 G. Li, D. Zhang, Q. Qiao, Y. Yu, D. Peterson, A. Zafar, R. Kumar, S. Curtarolo, F. Hunte, S. Shannon, Y. Zhu, W. Yang and L. Cao, *J. Am. Chem. Soc.*, 2016, **138**, 16632–16638.
75 X. J. Chua, S. M. Tan, X. Chia, Z. Sofer, J. Luxa and M. Pumera, *Chemistry*, 2017, **23**, 3169–3177.
76 T. F. Jaramillo, K. P. Jorgensen, J. Bonde, J. H. Nielsen, S. Horch and I. Chorkendorff, *Science*, 2007, **317**, 100–102.
77 M. Zheng, K. Guo, W.-J. Jiang, T. Tang, X. Wang, P. Zhou, J. Du, Y. Zhao, C. Xu and J.-S. Hu, *Appl. Catal. B Environ.*, 2019, **244**, 1004–1012.
78 A. Wang, K. Hu, Y. Liu, R. Li, C. Ye, Z. Yi and K. Yan, *Int. J. Hydrogen Energy*, 2019, **44**, 6573–6581.
79 H. Wang, X. Xiao, S. Liu, C. L. Chiang, X. Kuai, C. K. Peng, Y. C. Lin, X. Meng, J. Zhao, J. Choi, Y. G. Lin, J. M. Lee and L. Gao, *J. Am. Chem. Soc.*, 2019, **141**, 18578–18584.
80 L. Song, M. Zhao, X. Li, Z. Zhang and L. Qu, *RSC Adv.*, 2016, **6**, 70740–70746.
81 L. Zhang, J. Dong and F. Ding, *Chem. Rev.*, 2021, **10**, 191–199.
82 K. C. Kwon, T. H. Lee, S. Choi, K. S. Choi, S. O. Gim, S.-R. Bae, J.-L. Lee, H. W. Jang and S. Y. Kim, *Appl. Surf. Sci.*, 2021, **541**, 354–363.
83 K. H. Choi, S. Oh, S. Chae, B. J. Jeong, B. J. Kim, J. Jeon, S. H. Lee, S. O. Yoon, C. Woo, X. Dong, A. Ghulam, C. Lim, Z. Liu, C. Wang, A. Junaid, J.-H. Lee, H. K. Yu and J.-Y. Choi, *J. Alloys Compd.*, 2021, **853**, 576–585.
84 S. Dolai, P. Maiti, A. Ghorai, R. Bhunia, P. K. Paul and D. Ghosh, *ACS Appl. Mater. Interfaces*, 2021, **13**, 438–448.
85 F. Yang, Z. Cao, J. Wang, S. Wang and H. Zhong, *J. Alloys Compd.*, 2020, **817**, 678–691.
86 Y. Qiao, T. Hirtz, F. Wu, G. Deng, X. Li, Y. Zhi, H. Tian, Y. Yang and T.-L. Ren, *ACS Appl. Electron. Mater.*, 2019, **2**, 346–370.
87 Y. Yu, G. S. Jung, C. Liu, Y. C. Lin, C. M. Rouleau, M. Yoon, G. Eres, G. Duscher, K. Xiao, S. Irle, A. A. Puretzky and D. B. Geohegan, *ACS Nano*, 2021, **15**, 4504–4517.
88 X. Lin, F. Wang, X. Shan, Y. Miao, X. Chen, M. Yan, L. Zhang, K. Liu, J. Luo and K. Zhang, *Appl. Surf. Sci.*, 2021, **546**, 45–55.
89 S. Li, S. Tian, Y. Yao, M. He, L. Chen, Y. Zhang and J. Zhai, *Nanomaterials*, 2021, **11**, 98–108.
90 H. Sun, H. Liu, M. Nie, Z. Zhao, Z. Xue, J. Liao, F. Xue, S. Zhang, M. Wu and T. Gao, *Ceram. Int.*, 2021, **47**, 13994–14000.
91 Z. Zhang, W. Li, R. Wang, H. Li, J. Yan, Q. Jin, P. Feng, K. Wang and K. Jiang, *J. Alloys Compd.*, 2021, **872**, 389–399.
92 Z. Guo, W. Li, Y. He, G. Li, K. Zheng and C. Xu, *Appl. Surf. Sci.*, 2020, **512**, 576–587.
93 Y. Cai, H. Kang, F. Jiang, L. Xu, Y. He, J. Xu, X. Duan, W. Zhou, X. Lu and Q. Xu, *Appl. Surf. Sci.*, 2021, **546**, 1303–1314.
94 S. Jana, S. Kumar Bhar, N. Mukherjee and A. Mondal, *Mater. Lett.*, 2013, **109**, 51–54.
95 Y. Zhou, L. Jia, T. Wang, Y. Du and C. Wang, *Int. J. Hydrogen Energy*, 2018, **43**, 7356–7365.
96 K. Hernandez Ruiz, M. Ciprian, R. Tu, F. Verpoort, M. Li, S. Zhang, J. R. Vargas Garcia, H. Li, T. Goto, Y. Fan, W. Jiang and L. Zhang, *J. Alloys Compd.*, 2019, **806**, 1276–1284.
97 S. Kang, J.-J. Koo, H. Seo, Q. T. Truong, J. B. Park, S. C. Park, Y. Jung, S.-P. Cho, K. T. Nam, Z. H. Kim and B. H. Hong, *J. Mater. Chem. C*, 2019, **7**, 10173–10178.
98 I. Yang, S. Kim, M. Niihori, A. Alabadla, Z. Li, L. Li, M. N. Lockrey, D.-Y. Choi, I. Aharonovich, J. Wong-Leung, H. H. Tan, C. Jagadish and L. Fu, *Nano Energy*, 2020, **71**, 235–245.
99 Y. Feng, X. Wu, L. Hu and G. Gao, *J. Mater. Chem. C*, 2020, **8**, 14353–14359.
100 W. Wan, L. Zhan, B. Xu, F. Zhao, Z. Zhu, Y. Zhou, Z. Yang, T. Shih and W. Cai, *Small*, 2017, **13**, 465–475.
101 W. Wan, X. Li, X. Li, B. Xu, L. Zhan, Z. Zhao, P. Zhang, S. Q. Wu, Z.-z. Zhu, H. Huang, Y. Zhou and W. Cai, *RSC Adv.*, 2016, **6**, 323–330.
102 L. Li, X. Wang, J. Li, Y. Guo, X. Li and Y. Lu, *J. Alloys Compd.*, 2021, **872**, 892–902.
103 S. Y. Ding, M. Dong, Y. W. Wang, Y. T. Chen, H. Z. Wang, C. Y. Su and W. Wang, *J. Am. Chem. Soc.*, 2016, **138**, 3031–3037.

104 Z. Yuan, H.-J. Peng, J.-Q. Huang, X.-Y. Liu, D.-W. Wang, X.-B. Cheng and Q. Zhang, *Adv. Funct. Mater.*, 2014, **24**, 6105–6112.
105 X. Zhuang, Y. Mai, D. Wu, F. Zhang and X. Feng, *Adv. Mater.*, 2015, **27**, 403–427.
106 X. Wu, F. Tian, W. Wang, J. Chen, M. Wu and J. X. Zhao, *J. Mater. Chem. C*, 2013, **1**, 4676–4684.
107 J. Hicks, A. Tejeda, A. Taleb-Ibrahimi, M. S. Nevius, F. Wang, K. Shepperd, J. Palmer, F. Bertran, P. Le Fèvre, J. Kunc, W. A. de Heer, C. Berger and E. H. Conrad, *Nat. Phys.*, 2012, **9**, 49–54.
108 I. Bilecka and M. Niederberger, *Nanoscale*, 2010, **2**, 1358–1374.
109 L. Mai, L. Xu, C. Han, X. Xu, Y. Luo, S. Zhao and Y. Zhao, *Nano Lett.*, 2010, **10**, 4750–4755.
110 M. Yoshimura and K. Byrappa, *J. Mater. Sci.*, 2007, **43**, 2085–2103.
111 J. Jiang, Y. Li, J. Liu and X. Huang, *Nanoscale*, 2011, **3**, 45–58.
112 Y. Yang, H. Meng, S. Yan, H. Zhu, W. Ma, C. Wang, F. Ma and Z. Hu, *J. Alloys Compd.*, 2021, **874**, 677–687.
113 C. Ayappan, B. Palanivel, V. Jayaraman and A. Mani, *J. Alloys Compd.*, 2021, **871**, 1254–1264.
114 D. Lee, H. W. Lee, S. Mathur and K. H. Kim, *J. Alloys Compd.*, 2021, **868**, 1365–1375.
115 Y. Qiu, X. Zhang, H. Han, Z. Liu, J. Liu and X. Ji, *J. Power Sources*, 2021, **499**, 566–576.
116 N. Liu, L. Yang, S. Wang, Z. Zhong, S. He, X. Yang, Q. Gao and Y. Tang, *J. Power Sources*, 2015, **275**, 588–594.
117 D. Wang, X. Zhang, S. Bao, Z. Zhang, H. Fei and Z. Wu, *J. Mater. Chem. A*, 2017, **5**, 2681–2688.
118 C. Qin, A. Fan, X. Zhang, S. Wang, X. Yuan and X. Dai, *J. Mater. Chem. A*, 2019, **7**, 27594–27602.
119 M. Li, B. Cai, R. Tian, X. Yu, M. B. H. Breese, X. Chu, Z. Han, S. Li, R. Joshi, A. Vinu, T. Wan, Z. Ao, J. Yi and D. Chu, *Chem. Eng. J.*, 2021, **409**, 465–476.
120 Y. Xiao, M. Tan, Z. Li, L. He, B. Gao, Y. Chen, Y. Zheng and B. Lin, *Int. J. Hydrogen Energy*, 2021, **46**, 11688–11700.
121 W. Ding and X. Meng, *J. Alloys Compd.*, 2021, **866**, 2307–2317.
122 M. Kang, H. J. Chai, H. B. Jeong, C. Park, I. Y. Jung, E. Park, M. M. Cicek, I. Lee, B. S. Bae, E. Durgun, J. Y. Kwak, S. Song, S. Y. Choi, H. Y. Jeong and K. Kang, *ACS Nano*, 2021, **15**, 8715–8723.
123 Y. Liu, J. He, N. Zhang, W. Zhang, Y. Zhou and K. Huang, *J. Mater. Sci.*, 2021, **56**, 12559–12583.
124 W. T. Kang, T. L. Phan, K. J. Ahn, I. Lee, Y. R. Kim, U. Y. Won, J. E. Kim, Y. H. Lee and W. J. Yu, *ACS Appl. Mater. Interfaces*, 2021, **13**, 18056–18064.
125 Y.-H. Ting, M.-C. Wu, Y. Aoyama, K.-C. Lu and W.-W. Wu, *Appl. Surf. Sci.*, 2021, **544**, 809–819.
126 S. D. Thammaiah, X. Liu, T. Knežević, K. M. Batenburg, A. A. I. Aarnink and L. K. Nanver, *Solid-State Electron.*, 2021, **177**, 763–773.
127 J. Wen, Y. Wan, Y. Dong, H. Zhan, Y. Luo, F. Tang, G. D. West, F. Pang, G. Peng and T. Wang, *J. Lumin.*, 2021, **231**, 689–699.
128 B. Shi, D. Zhou, R. Qiu, M. Bahri, X. Kong, H. Zhao, C. Tlili and D. Wang, *Appl. Surf. Sci.*, 2020, **533**, 1567–1577.
129 M. P. Browne, F. Novotný, C. L. Manzanares Palenzuela, J. Šturala, Z. Sofer and M. Pumera, *ACS Sustainable Chem. Eng.*, 2019, **7**, 16440–16449.
130 S. H. Yu, Z. Tang, Y. Shao, H. Dai, H. Y. Wang, J. Yan, H. Pan and D. H. C. Chua, *ACS Appl. Energy Mater.*, 2019, **2**, 5799–5808.
131 G. Fiori, F. Bonaccorso, G. Iannaccone, T. Palacios, D. Neumaier, A. Seabaugh, S. K. Banerjee and L. Colombo, *Nat. Nanotechnol.*, 2014, **9**, 768–779.
132 L. K. Tan, B. Liu, J. H. Teng, S. Guo, H. Y. Low and K. P. Loh, *Nanoscale*, 2014, **6**, 14002–14012.
133 R. F. Frindt, *J. Appl. Phys.*, 1966, **37**, 1928–1929.
134 X. Wu, M. Yu, J. Liu, Y. Ma and S. Li, *Chem. Eng. J.*, 2020, **381**, 189–201.
135 L. Zhang and X. W. Lou, *Chemistry*, 2014, **20**, 5219–5223.
136 Z. Zeng, Z. Yin, X. Huang, H. Li, Q. He, G. Lu, F. Boey and H. Zhang, *Angew. Chem., Int. Ed.*, 2011, **50**, 11093–11097.
137 J. N. Coleman, M. Lotya, A. O'Neill, S. D. Bergin, P. J. King, U. Khan, K. Young, A. Gaucher, S. De, R. J. Smith, I. V. Shvets, S. K. Arora, G. Stanton, H. Y. Kim, K. Lee, G. T. Kim, G. S. Duesberg, T. Hallam, J. J. Boland, J. J. Wang, J. F. Donegan, J. C. Grunlan, G. Moriarty, A. Shmeliov, R. J. Nicholls, J. M. Perkins, E. M. Grieveson, K. Theuwissen, D. W. McComb, P. D. Nellist and V. Nicolosi, *Science*, 2011, **331**, 568–571.
138 R. A. Frampton, C. Taylor, A. V. Holguin Moreno, S. B. Visnovsky, N. K. Petty, A. R. Pitman and P. C. Fineran, *Appl. Environ. Microbiol.*, 2014, **80**, 2216–2228.
139 K. G. Zhou, N. N. Mao, H. X. Wang, Y. Peng and H. L. Zhang, *Angew. Chem., Int. Ed.*, 2011, **50**, 10839–10842.
140 A. S. Aliyev, M. Elrouby and S. F. Cafarova, *Mater. Sci. Semicond. Process.*, 2015, **32**, 31–39.
141 X. Ping, W. Liu, Y. Wu, G. Xu, F. Chen, G. Li and L. Jiao, *Adv. Mater.*, 2022, **2**, 484–494.
142 J. H. Hwang, S. Fahad, H. Ryu, K. L. Rodriguez, J. S. Domingo, A. Kushima and W. H. Lee, *J. Power Sources*, 2022, **527**, 1–11.
143 L. E. Strange, S. Garg, P. Kung, M. Ashaduzzaman, G. Szulczewski and S. Pan, *J. Electrochem. Soc.*, 2022, **169**, 574–584.
144 J. Jiang, H. Cong, X. Huang, R. Sun, Y. Li, W. Xu, H. Wang and S. Han, *Int. J. Hydrogen Energy*, 2022, **47**, 2947–2957.
145 D. G. Li, D. R. Chen and P. Liang, *J. Alloys Compd.*, 2021, **873**, 901–911.
146 D. Chen, X. Zhan, T. Liu, Y. Zhao, N. Qi and L. Sun, *Opt Laser. Technol.*, 2021, **140**, 809–819.
147 Q. Wang, X. Kong, Y. Yu, H. Han, G. Sang, G. Zhang, Y. Yi and T. Gao, *J. Nucl. Mater.*, 2021, **551**, 532–542.
148 X. Wang, J. Wang, B. Wei, N. Zhang, J. Xu, H. Miao, L. Liu, C. Su, Y. Li and Z. Wang, *J. Mater. Sci. Technol.*, 2021, **78**, 170–175.
149 E. P. C. Higgins, A. A. Papaderakis, C. Byrne, A. S. Walton, D. J. Lewis and R. A. W. Dryfe, *Electrochim. Acta*, 2021, **382**, 570–581.

150 J. Li, C. Zhang, H. Ma, T. Wang, Z. Guo, Y. Yang, Y. Wang and H. Ma, *Chem. Eng. J.*, 2021, **414**, 1265–1275.
151 Y. Du, H. Zhao, W. Wang, X. Jiang, Y. Yang, Y. Liu, S. Li and L. Wang, *J. Solid State Chem.*, 2021, **296**, 3045–3055.
152 G. Liu, J. Li, C. Dong, L. Wu, D. Liang, H. Cao and P. Lu, *Int. J. Hydrogen Energy*, 2021, **46**, 18294–18304.
153 W. Zhou, L. Dong, L. Tan and Q. Tang, *Nanotechnology*, 2021, **32**, 145718.
154 J. Tang, Y. Chu, K. Wang, B. Deng, Y. Li and X. Tan, *ACS Appl. Energy Mater.*, 2021, **4**, 2300–2306.
155 N. Ran, B. Sun, W. Qiu, E. Song, T. Chen and J. Liu, *J. Phys. Chem. Lett.*, 2021, **12**, 2102–2111.
156 W. Dong, H. Liu, X. Liu, H. Wang, X. Li and L. Tian, *Int. J. Hydrogen Energy*, 2021, **46**, 9360–9370.
157 Y. Dai, X. Wang, P. Wang, Y. Sun, R. Han and C. Luo, *Int. J. Hydrogen Energy*, 2021, **46**, 6419–6426.
158 Y. Kang, *Surf. Sci.*, 2021, **704**, 468–478.
159 Y. Li, Z. Yin, M. Cui, X. Liu, J. Xiong, S. Chen and T. Ma, *J. Mater. Chem. A*, 2021, **9**, 2070–2092.
160 S. Bolar, S. Shit, N. C. Murmu, P. Samanta and T. Kuila, *ACS Appl. Mater. Interfaces*, 2021, **13**, 765–780.
161 J. Wu, B. Sun, H. Wang, Y. Li, Y. Zuo, W. Wang, H. Lin, S. Li and L. Wang, *J. Mater. Chem. A*, 2021, **9**, 482–491.
162 M. Wang, R. Song, X. Zhang, G. Liu, S. Xu, Z. Xu, J. Liu and G. Qiao, *Int. J. Hydrogen Energy*, 2021, **46**, 1913–1922.
163 J. Lee, J. Heo, H. Y. Lim, J. Seo, Y. Kim, J. Kim, U. Kim, Y. Choi, S. H. Kim, Y. J. Yoon, T. J. Shin, J. Kang, S. K. Kwak, J. Y. Kim and H. Park, *ACS Nano*, 2020, **14**(12), 17114–17124.
164 Y. Du, W. Wang, H. Zhao, Y. Liu, S. Li and L. Wang, *J. Mater. Chem. A*, 2020, **8**, 25165–25172.
165 L. Zeng, X. Li, S. Fan, Z. Yin, J. Mu, M. Qin and A. Chen, *J. Power Sources*, 2020, **478**, 564–578.
166 F. Sun, A. Hong, W. Zhou, C. Yuan and W. Zhang, *Mater. Today Commun.*, 2020, **25**, 3092–3103.
167 I. Matanovic, K. Leung, S. J. Percival, J. E. Park, P. Lu, P. Atanassov and S. S. Chou, *Appl. Mater. Today*, 2020, **21**, 328–332.
168 Y. Li, S. Zuo, Q. H. Li, X. Wu, J. Zhang, H. Zhang and J. Zhang, *Nano Lett.*, 2021, **21**, 1848–1855.
169 X. Wang, Y. Zhang, H. Si, Q. Zhang, J. Wu, L. Gao, X. Wei, Y. Sun, Q. Liao, Z. Zhang, K. Ammarah, L. Gu, Z. Kang and Y. Zhang, *J. Am. Chem. Soc.*, 2020, **142**, 4298–4308.
170 S. Park, S. Siahrostami, J. Park, A. H. B. Mostaghimi, T. R. Kim, L. Vallez, T. M. Gill, W. Park, K. E. Goodson, R. Sinclair and X. Zheng, *Adv. Mater.*, 2020, **32**, 3020–3031.
171 Z. Zhang, H. Zhu, J. Hao, S. Lu, F. Duan, F. Xu and M. Du, *J. Colloid Interface Sci.*, 2021, **595**, 88–97.
172 Q. Wu, A. Dong, C. Yang, L. Ye, L. Zhao and Q. Jiang, *Chem. Eng. J.*, 2021, **413**, 3001–3012.
173 J. Wu, X. Wang, J. Jiang, W. Lin, S. Zhu, J. Sha, L. Ma and N. Zhao, *Mater. Lett.*, 2021, **292**, 309–324.
174 M. Wang, J. Yang, X. You, C. Liao, J. Yan, J. Ruan and S. Dong, *J. Mater. Sci. Technol.*, 2021, **71**, 23–30.
175 Y. Huang, J. Lv, J. Huang, K. Xu and L. Liu, *Nanotechnology*, 2021, **32**, 5602–5615.
176 H. R. Inta, S. Ghosh, A. Mondal, G. Tudu, H. V. S. R. M. Koppisetti and V. Mahalingam, *ACS Appl. Energy Mater.*, 2021, **4**, 2828–2837.
177 X. Song, B. Li, W. Peng, C. Wang, K. Li, Y. Zhu and Y. Mei, *Nanoscale*, 2021, **13**, 5892–5900.
178 B. Zhang, K. Xu, X. Fu, S. Guan, X. Li and Z. Peng, *J. Alloys Compd.*, 2021, **856**, 3002–3015.
179 B. Zhang, J. Li, Q. Song, X. Xu, W. Hou and H. Liu, *Inorg. Chem.*, 2021, **60**, 2604–2613.
180 R. Narasimman, M. Waldiya, K. Jalaja, S. K. Vemuri, I. Mukhopadhyay and A. Ray, *Int. J. Hydrogen Energy*, 2021, **46**, 7759–7771.
181 Z. Chen, X. Liu, P. Xin, H. Wang, Y. Wu, C. Gao, Q. He, Y. Jiang, Z. Hu and S. Huang, *J. Alloys Compd.*, 2021, **853**, 4651–4663.
182 Q. Wei, Z. Ye, X. Ren, X. Li, M. Yin, L. Zan and F. Fu, *J. Alloys Compd.*, 2020, **835**, 5890–5903.
183 Y. Mei, T. T. Li, J. Qian, H. Li, M. Wu and Y. Q. Zheng, *Chem. Commun.*, 2020, **56**, 13393–13396.
184 Q. He, S. Huang, M. Liu, P. Li, W. Sun and L. Hou, *Inorg. Chem. Front.*, 2020, **7**, 2660–2668.
185 H. Huang, J. Song, D. Yu, Y. Hao, Y. Wang and S. Peng, *Appl. Surf. Sci.*, 2020, **525**, 4309–4313.
186 A. Tahira, Z. H. Ibupoto, R. Mazzaro, S. You, V. Morandi, M. M. Natile, M. Vagin and A. Vomiero, *ACS Appl. Energy Mater.*, 2019, **2**, 2053–2062.
187 B. Cao, G. M. Veith, J. C. Neuefeind, R. R. Adzic and P. G. Khalifah, *J. Am. Chem. Soc.*, 2013, **135**, 19186–19192.
188 A. Tahira, Z. H. Ibupoto, R. Mazzaro, S. You, V. Morandi, M. M. Natile, M. Vagin and A. Vomiero, *ACS Appl. Energy Mater.*, 2019, **2**, 2053–2062.
189 Y. Wang, F. Lu, K. Su, N. Zhang, Y. Zhang, M. Wang and X. Wang, *Chem. Eng. J.*, 2020, **399**, 5901–5915.
190 M. Yan, Q. Jiang, L. Yang, H. He and H. Huang, *ACS Appl. Energy Mater.*, 2020, **3**, 6880–6888.
191 A. Wu, Y. Gu, Y. Xie, H. Yan, Y. Jiao, D. Wang and C. Tian, *J. Alloys Compd.*, 2021, **867**, 3907–3917.
192 S. Liu, S. Li, K. Sekar, R. Li, Y. Zhu, R. Xing, K. Nakata and A. Fujishima, *Int. J. Hydrogen Energy*, 2019, **44**, 25310–25318.
193 Z. Liu, K. Wang, Y. Li, S. Yuan, G. Huang, X. Li and N. Li, *Appl. Catal. B Environ.*, 2022, **300**, 4821–4834.
194 Q. Xiong, X. Zhang, H. Wang, G. Liu, G. Wang, H. Zhang and H. Zhao, *Chem. Commun.*, 2018, **54**, 3859–3862.
195 Y. Zhao, K. Kamiya, K. Hashimoto and S. Nakanishi, *J. Am. Chem. Soc.*, 2015, **137**, 110–113.
196 G.-F. Chen, Y. Luo, L.-X. Ding and H. Wang, *ACS Catal.*, 2017, **8**, 526–530.
197 J. Y. Xue, F. L. Li, Z. Y. Zhao, C. Li, C. Y. Ni, H. W. Gu, D. J. Young and J. P. Lang, *Inorg. Chem.*, 2019, **58**, 11202–11209.
198 C. Wang, *Int. J. Electrochem. Sci.*, 2019, **66**, 11607–11615.
199 T. H. M. Lau, X. Lu, J. Kulhavy, S. Wu, L. Lu, T. S. Wu, R. Kato, J. S. Foord, Y. L. Soo, K. Suenaga and S. C. E. Tsang, *Chem. Sci.*, 2018, **9**, 4769–4776.

200 Q. Xiong, Y. Wang, P. F. Liu, L. R. Zheng, G. Wang, H. G. Yang, P. K. Wong, H. Zhang and H. Zhao, *Adv. Mater.*, 2018, 1450–1461, DOI: **10.1002/adma.201801450**.
201 B. Gao, X. Du, Y. Ma, Y. Li, Y. Li, S. Ding, Z. Song and C. Xiao, *Appl. Catal. B Environ.*, 2020, **263**, 3769–3779.
202 J. Huang, M. Chen, T. Tang, W. Liu and Y. Liu, *Electrochim. Acta*, 2020, **355**, 6751–6764.
203 Z. Luo, Y. Ouyang, H. Zhang, M. Xiao, J. Ge, Z. Jiang, J. Wang, D. Tang, X. Cao, C. Liu and W. Xing, *Nat. Commun.*, 2018, **9**, 2120–2130.
204 X. Sun, J. Dai, Y. Guo, C. Wu, F. Hu, J. Zhao, X. Zeng and Y. Xie, *Nanoscale*, 2014, **6**, 8359–8367.
205 J. Zhang, X. Xu, L. Yang, D. Cheng and D. Cao, *Small Methods*, 2019, **3**, 932–942.
206 X. Y. Yu, Y. Feng, Y. Jeon, B. Guan, X. W. Lou and U. Paik, *Adv. Mater.*, 2016, **28**, 9006–9011.
207 J. Yu, Q. He, G. Yang, W. Zhou, Z. Shao and M. Ni, *ACS Catal.*, 2019, **9**, 9973–10011.
208 J. Ge, D. Zhang, Y. Qin, T. Dou, M. Jiang, F. Zhang and X. Lei, *Appl. Catal. B Environ.*, 2021, **298**, 8012–8024.
209 D. Wang, Y. Xie and Z. Wu, *Nanotechnology*, 2019, **30**, 401–413.
210 Y. Deng, Z. Liu, A. Wang, D. Sun, Y. Chen, L. Yang, J. Pang, H. Li, H. Li, H. Liu and W. Zhou, *Nano Energy*, 2019, **62**, 338–347.
211 J. Liu, Z. Wang, J. Li, L. Cao, Z. Lu and D. Zhu, *Small*, 2020, **16**, 738–748.
212 T. Wang, X. Zhang, P. Yang and S. P. Jiang, *Inorg. Chem. Front.*, 2020, **7**, 3578–3587.
213 J. Tian, N. N. Xia and C. Lin, *Int. J. Energy Res.*, 2021, **45**, 8639–8647.
214 X. Meng, L. Yu, C. Ma, B. Nan, R. Si, Y. Tu, J. Deng, D. Deng and X. Bao, *Nano Energy*, 2019, **61**, 611–616.
215 Z. Wu, X. Guo, Z. Zhang, M. Song, T. Jiao, Y. Zhu, J. Wang and X. Liu, *ACS Sustainable Chem. Eng.*, 2019, **7**, 16577–16584.
216 Y. Sun, Y. Zang, W. Tian, X. Yu, J. Qi, L. Chen, X. Liu and H. Qiu, *Energy Environ. Sci.*, 2022, **3**, 825–836.
217 A. E. Russell, *Faraday Discuss.*, 2008, **140**, 9–10.
218 A. Shan, X. Teng, Y. Zhang, P. Zhang, Y. Xu, C. Liu, H. Li, H. Ye and R. Wang, *Nano Energy*, 2022, 94.
219 J. Zhang, T. Wang, D. Pohl, B. Rellinghaus, R. Dong, S. Liu, X. Zhuang and X. Feng, *Angew. Chem., Int. Ed.*, 2016, **55**, 6702–6707.
220 C. Tsai, F. Abild-Pedersen and J. K. Norskov, *Nano Lett.*, 2014, **14**, 1381–1387.
221 I. S. Amiinu, Z. Pu, X. Liu, K. A. Owusu, H. G. R. Monestel, F. O. Boakye, H. Zhang and S. Mu, *Adv. Funct. Mater.*, 2017, **27**, 553–564.
222 G. Zhang, H. Liu, J. Qu and J. Li, *Energy Environ. Sci.*, 2016, **9**, 1190–1209.